PHYSICAL REVIEW B VOLUME 56, NUMBER 10 1 SEPTEMBER 1997-II

In-plane surface impedance of epitaxial $YBa_2Cu_3O_{7-\delta}$ films: Comparison of experimental data taken at 87 GHz with *d*- and *s*-wave models of superconductivity

S. Hensen and G. Müller
Fachbereich Physik, Universität Wuppertal, Gaußstrasse 20, D-42097 Wuppertal, Germany

C. T. Rieck and K. Scharnberg
Fachbereich Physik, Universität Hamburg, Jungiusstrasse 11, D-20355 Hamburg, Germany

(Received 29 January 1997)

We have measured the temperature dependence of both the surface resistance and the change of the penetration depth in two optimized epitaxial *c*-axis oriented $YBa_2Cu_3O_{7-\delta}$ (YBCO) films at 87 GHz by incorporating each film as an end plate in a cylindrical copper cavity. A high frequency is used in order to increase losses in the superconducting samples relative to the losses in the copper cavity. It is found that our measuring frequency is of a magnitude comparable to the relevant low-temperature scattering rates, so that the real part of the conductivity would be expected to display significant frequency dependence. The two films investigated were both 350 nm thick, but prepared by different techniques. The experimental results are compared to weak-coupling *d*- and *s*-wave models of superconductivity which incorporate both inelastic and elastic scattering, with the latter forming a small part of the total scattering. The sizable surface resistance at low temperatures and the approximately linear temperature variation can be accounted for without subtracting an extrinsic residual surface resistance, if *d*- or anisotropic *s*-wave order parameters with nearly vanishing Fermi surface averages and scattering phase shifts close to 0.4π are assumed. Large low-temperature losses are obtained theoretically in spite of the fact that order parameter amplitudes must be in the range of $2\Delta_0(0)/k_BT_c = 6.0–7.5$, considerably larger than the corresponding weak-coupling values, in order to describe the data at higher temperatures. When inelastic scattering is represented by a phenomenological temperature-dependent scattering rate, a quantitative fit to the experimental data for both the surface resistance and the penetration depth of YBCO over the whole measured temperature range from 4.2 to 145 K can be obtained within a single model. Some discrepancy between theory and experiment remains near the transition temperature where fluctuation effects, not treated in this paper, are clearly visible. While very different parameter sets can be found that would fit the real part of the conductivity, having to explain both penetration depth and surface resistance puts severe constraints on the available parameter space. A description of the inelastic scattering on the basis of spin fluctuation exchange within the nested Fermi-liquid model with full frequency dependence taken into account still gives reasonable fits to the data, even though only a single parameter, fixed by the normal-state resistivity, is involved. For *s*-wave states, whose Fermi surface average is a sizable fraction of the order-parameter amplitude, scattering rates drop well below the experimental frequency at sufficiently low temperatures for the whole range of scattering phase shifts. Thermally excited quasiparticles still present then act as a nearly ideally conducting system which results in losses too low to be compatible with the experimental observations. [S0163-1829(97)10034-0]

I. INTRODUCTION

Since the first microwave surface impedance measurements of epitaxial $YBa_2Cu_3O_{7-\delta}$ (YBCO) films,[1,2] which were found to have significantly lower microwave losses than granular samples,[3] it has become clear that even optimized films[4–7] of oxide superconductors available at the present time exhibit much higher microwave losses at low temperatures than conventional superconductors at the same reduced temperature T/T_c.[8,9] Various attempts have been made to describe the temperature-dependent microwave surface impedance of YBCO theoretically in terms of intrinsic material properties. These include, e.g., modified two-fluid models,[3,10] single-gap *s*-wave BCS approaches,[11,12] two-band, two-gap models based on *s*-wave BCS theory[13] with generalizations to include strong-coupling effects,[14–18] and models based on *d*-wave pairing symmetry.[19–22] For a recent review see Ref. 23. So far these models have failed to account satisfactorily for the observed residual surface resistance and the linear variation of the surface resistance with temperature up to around half the transition temperature.[24] Unless these models can be suitably refined, the remaining discrepancies must be attributed to extrinsic effects resulting from random extended defects, which at present can only be described phenomenologically.[9,12,25] Such extrinsic effects would be strongly sample dependent.

A range of highly sophisticated preparation techniques has been developed in recent years yielding high-quality YBCO thin films with very similar microwave properties,[4–6] which are also similar to those of high-quality single crystals.[19,20,26,27] Moreover, YBCO films comparable to those investigated in this work did not show any power dependence of the electromagnetic response up to field levels $>10^4$A/m at 4.2 K.[5,7] In contrast, low quality samples regularly display a power dependence of the ac response at considerably lower fields and an increased penetration depth, which are attributed to weak links.[8,25] The linearity of the current-field relationship extending up to comparatively high fields tallies with the observation of high critical currents in these films. All these points convinced us that, as in the single-crystal work,[19,20,26,27] we are observing intrinsic effects in optimized YBCO films closely related to the superconducting pair state present in YBCO, in spite of the fact that the films are heavily twinned.

In single crystals it is possible to remove twin boundaries which, one would hope, would reveal their contribution to the microwave losses. Such work has been undertaken by the UBC group[26] but, as the comparison between Ref. 26, Fig. 4 and Ref. 28, Fig. 3 shows, the results are not clear cut. At a lower experimental frequency of 4.13 GHz detwinning has a rather small effect on the surface resistance. Twins appear to suppress the peak in R_s at intermediate temperatures in much the same way as the addition of Ni or Zn impurities.[26] It is only at the lowest temperatures that R_s appears to be reduced by detwinning. This is consistent with the picture that twin boundaries are regions of finite width in which the lattice is strongly disordered[29] and hence contribute to the elastic scattering of charge carriers. At a higher experimental frequency of 34.8 GHz detwinning reduces R_s at all temperatures and particularly so at low temperatures. There seems to be no simple explanation why detwinning should have a different effect on R_s at different frequencies.

We have performed measurements of the microwave surface impedance as a function of temperature on the YBCO films using an end-plate replacement technique with a cylindrical copper cavity at 87 GHz, which offers a high measurement sensitivity for both the surface resistance and changes of the penetration depth, as detailed in Sec. II. Unfortunately, the absolute value of the penetration depth λ in the superconducting state cannot be measured directly with this technique. The London penetration depth does not only serve as a useful indicator of sample quality, it also plays an important role in the comparison between theory and experiment. However, in view of the similarity between the surface impedance measured on our epitaxial films and the results obtained on single crystals we believe our films to be of similar quality with variations in the London penetration depth too small to be resolved by either μSR,[30] FIR reflectivity,[31] coplanar resonator measurements,[32] or microwave transmission measurements.[33–35] We shall analyze the effect a moderate change in the assumed London penetration depth has on the interpretation of the data.

As already mentioned, the microwave losses at low temperatures are much higher in YBCO than in conventional superconductors. They are incompatible with the notion of an energy gap, as is the nonexponential approach of the penetration depth to its zero temperature limit. Such behavior of the surface impedance has been discussed extensively in the context of heavy fermion superconductivity where it has been attributed to unconventional pairing.[36,37] Based on the perceived importance of spin fluctuations in high-T_c materials, on their layered structure, and on their complex band structure, a wide range of superconducting pair states have been proposed,[38] all of which differ significantly from the BCS result with its isotropic energy gap. In the present paper we shall restrict the comparison between experiment and theory to two-dimensional models designed to describe the conductivity of the CuO_2 planes. This restriction appears to be well justified because in our experimental arrangement there is no current flowing parallel to the c axis. To account for the apparent absence of an energy gap we focus on a d-wave model for the pair state, which is supported by other experiments[39,40] and which would follow rather naturally from a spin fluctuation mechanism of superconductivity.[41–44] Objections have been raised against the ability of this mechanism to account for the high transition temperatures[45] and a more likely scenario appears to be a concatenation of various effects, including electron-phonon interaction,[46,47] which could, nonetheless, favor d-wave superconductivity.[47,48]

The most prominent feature of a d-wave state that sets it apart from commonly considered anisotropic s-wave states is the change of sign of the order parameter as the relative momentum of the two quasiparticles forming a Cooper pair varies across the Brillouin zone. The electromagnetic response in the local limit is not sensitive to such a sign change[49] so that we do not expect to find qualitative differences between anisotropic s-wave and d-wave superconductors in the clean limit. Scattering processes affect these two types of states differently, though,[50,51] and it has been suggested that a comparison of results obtained at different doping levels will provide some clue as to the exact nature of the pair state.[52,53] The analysis presented in this paper shows that small amounts of elastic scattering unavoidable in these complex materials are sufficient to eliminate from the discussion states with nodes in the energy gap but without a sign change in the order parameter. The symmetry of the order parameter, actually, cannot be determined by doping experiments because an anisotropic s-wave state whose Fermi surface average vanishes[38] can give results identical to those of a d-wave state. Some experimental tests that are sensitive to the sign of the order parameter can be taken as evidence for d-wave symmetry while there is no experimental evidence for anisotropic s-wave states with four nodal lines.[38] So far, these experiments[39,40,54] are still somewhat controversial, but the case in favor of d-wave superconductivity appears to grow stronger.[39,40] Even c-axis tunneling now seems to support the notion that the order parameter is predominantly d wave in character with a small s-wave contribution,[55] consistent with the orthorhombic symmetry of YBCO.

The importance of the presence of some small amount of elastic scattering characterized by a normal-state scattering rate Γ_N^{el} and the strength of the individual scatterer parametrized by the s-wave scattering phase shift δ_N has already been mentioned. We only consider s-wave scattering in order to keep the number of parameters down. Inspection of the normal-state conductivity of high-T_c materials shows that inelastic-scattering processes must also be important which, in view of the high transition temperature, is not surprising. Whether the interaction responsible for this inelastic scattering is also the source of the pairing interaction is not clear. Calculating both the superconducting properties and the normal-state electromagnetic response from the same interaction is not too difficult for isotropic systems. With the elastic scattering making a negligible contribution to the resistivity ρ_n above the transition temperature T_c, one faces the problem of having to explain both T_c and $\rho_n(T)$ with the same set of parameters. This is impossible in most cases and the momentum dependence of the interaction has been invoked to explain discrepancies between experiment and such an isotropic strong-coupling theory.[56,57] In the case of d-wave pairing the momentum dependence of the interaction is essential and a complete description of superconductivity and transport in YBCO would require a fully anisotropic strong-coupling theory including elastic scattering and band-structure effects. Attempting to calculate the electromagnetic response in the superconducting state from such a theory one soon reaches the limits of available computer capacity. Furthermore, the necessary input for such a theory has not yet been established beyond reasonable doubt. For these reasons we shall use a weak-coupling theory in which T_c appears as parameter.

The inelastic-scattering rate at T_c, $\Gamma^{\text{inel}}(T_c)$, is of the order of T_c and for a d-wave state would be expected to have a strong effect on T_c. We assume that this effect is already included in some microscopic theory of T_c. The elastic scattering required to fit the data turns out to be so small that its effect on T_c can be neglected.

The inelastic-scattering processes determining the electromagnetic response may not be responsible for superconductivity but they could nevertheless be strongly affected by the transition to the superconducting state. A dramatic reduction in the scattering rate below T_c has been deduced from surface impedance measurements by Bonn *et al.*[19,26] using a two-fluid model. We shall briefly discuss the merits and shortcomings of the two-fluid model in the context of d-wave superconductivity. A phenomenological temperature-dependent inelastic-scattering rate will be deduced from fits to the experimental data using the full theory. This approach neglects the inevitable frequency dependence involved in inelastic scattering. There exist several theoretical models for the inelastic scattering,[58,59] notably the *nested Fermi-liquid* (NFL) model proposed by Ruvalds *et al.*,[60] that include this frequency dependence. They describe the linear temperature dependence of the normal-state resistivity with a single parameter and yield scattering rates which decrease rapidly upon entry into the superconducting state. In this paper we use the nested Fermi-liquid model for a more microscopic model of inelastic scattering.

The theory developed in this paper contains some more simplifying assumptions not yet mentioned. The Fermi surface is taken to be cylindrical with circular cross section so that the Fermi velocity is constant. When this is generalized using model band structures some, rather limited, quantitative changes are found.[61] These, however, cannot be taken seriously without considering a momentum dependence of the scattering rate. The assumed in-plane isotropy is in disagreement with the a-b anisotropy of the surface impedance observed on untwinned single crystals.[62,31] Similar anisotropy has been found in the normal-state transport properties.[63] Preliminary measurements of the surface resistance of partially untwinned single crystals, which were rotated *in situ,* also revealed anisotropy. In this case, however, the anisotropy at low temperatures was found to be opposite to that in the normal state.[64]

The anisotropy of the in-plane penetration depth appears to be incompatible with the picture of proximity-induced superconductivity in the CuO-chains[65,66] because in the model used the order parameter actually vanishes over large parts of the chain Fermi surface. Judging from the similarity in the temperature dependence of the penetration depths in the a and b directions, order-parameter amplitudes on the chains and planes seem to be of similar magnitude[65,66] so that the superconducting state of the coupled system could be described simply in terms of an elliptic Fermi surface and an order parameter compatible with orthorhombic symmetry.[67] Our films are heavily twinned and tested by circular microwave currents so that this anisotropy is averaged out. In-plane anisotropy is also absent in the chain-plane model proposed by Kresin and Wolf[15,16] because the quasiparticle energy has been integrated out. The boson exchange between quasiparticles residing on the chains and plains, respectively, could lead to a large gap on the chains. To account for the observed gaplessness, magnetic scattering on the chains is introduced. So far, only the zero frequency penetration depth has been calculated within this model showing that in a narrow temperature range above $T=0$ various experimental data can be explained reasonably well by adjusting the magnetic-scattering rate.[68]

The feature that distinguishes this work from others in this field is that the comparison between theory and experiment includes two separate quantities measured independently, covers the whole temperature range 4.2 K$\leqslant T \leqslant$145 K in which experimental data have been taken, and extends to two samples prepared by different techniques. We emphasize the role of intermediate scattering phase shifts and that of the self-energy part χ, which renormalizes the quasiparticle energy.

II. EXPERIMENTAL TECHNIQUES

A. Preparation and structural quality of YBCO films

We have investigated two c-axis oriented $YBa_2Cu_3O_{7-\delta}$ (YBCO) films, which were epitaxially grown on single-crystalline substrates by different deposition techniques. Both films were 10×10 mm^2 in size and their thicknesses were estimated from the deposition rates to be 350 nm. Sample A was grown by evaporation of the metals from three electron-beam heated sources in the presence of atomic oxygen. The technique is essentially as described in Refs. 69,70. The film was grown at a rate of 0.117 nm/s on a MgO substrate. The estimated oxygen pressure during film growth was $\sim 2\times10^{-2}$ Pa, with a significant fraction of atomic oxygen present. The sample was slowly cooled down and then annealed twice in molecular and once in atomic oxygen to optimize its oxygen content.[4] Sample B was prepared by high oxygen-pressure on-axis dc sputtering from a stoichiometric target as described in Refs. 71,72. It was grown on a $LaAlO_3$ substrate with a deposition rate of 0.018 nm/s. The oxygen pressure during growth was 385 Pa with a small amount of activated oxygen, as usually found in dc gas discharges in the pressure range of a few hundred Pa. The sample was slowly cooled down. Both deposition techniques have been optimized for films with low microwave losses. The two samples originate from systematic optimization series and are representative for the best films, i.e., those with the lowest residual losses and normal-state resistivities, of this series.

For sample A, a cation composition of 16.8% Y, 33.3% Ba, and 49.9% Cu was determined by accurate measurement of the evaporation rates, calibrated with careful microprobe energy dispersive x-ray (EDX) analysis, judiciously combined with morphology data.[4] The optimized sputtered films grown under the above mentioned conditions were generally found to contain (18.0±0.3)%Y, (32.0±0.3)% Ba, and (50.0±0.5)% Cu on a macroscopic average, as determined by Rutherford backscattering spectroscopy (RBS) measurements on several reference samples.[73] The transition temperatures T_c and critical current densities J_c of the YBCO films were measured by an inductive technique based on the detection of the third harmonic.[74] Superconductivity was found to set in at $T_c^A = 91.6$ K and $T_c^B = 90.5$ K with transition widths $\Delta T_c^A = 1.6$ K and $\Delta T_c^B = 0.4$ K. Results obtained for the critical current densities were $J_c(77\ \mathrm{K}) = 3.7$ MA/cm^2 and 3.1 MA/cm^2 for samples A and B, respectively. These large critical current densities indicate that defects acting as pinning centers for vortices introduced by the Earth's magnetic field and the self-field of the current do not show pronounced weak link behavior. Transition temperatures and critical current densities given here are typical values which can be reproducibly obtained by the two techniques.

Both samples were extensively characterized by x-ray diffraction: The c-axis lattice parameters were determined from the Bragg angle of the 006 line and found to be $c = 11.708 \pm 0.005$ Å for sample A and $c = 11.665 \pm 0.01$ Å for sample B. The full width at half maximum of the 006 line, which gives a measure of the nonuniformity of the c lattice parameter, was determined to be $\Delta c = \pm 0.019$ Å for sample A and $\Delta c = \pm 0.004$ Å for sample B. The rocking curve widths $\Delta\omega$ of the 006 line, which give a measure of the mosaic spread of the c-axis orientation over the sample, were 0.40° for sample A and 0.27° for sample B. No a-axis oriented material could be identified in either sample within the instrumental resolution. 45° in-plane misoriented material could not be detected in sample A while slight traces $<0.3\%$ of it were found in sample B. It is most remarkable that YBCO films with otherwise very comparable quality exhibit such a large difference in absolute c-axes lattice parameters and that the c-axis length of sample B is close to the low end of the spread found for bulk material.[75] Systematic investigation of the dependence of T_c and J_c on the c-axis length of comparable evaporated and sputtered YBCO films[4] revealed a similar, slightly overdoped oxygenation of both samples. The increased c-axis lattice parameter of sample A is believed to be related to a combination of higher cation disorder in this film and the difference in substrate materials.[4]

B. Surface impedance measurements

The surface impedance

$$Z_s(T,\omega) = R_s(T,\omega) - iX_s(T,\omega)$$
$$= R_s(T,\omega) - i\omega\mu_0\lambda(T,\omega) \tag{1}$$

of the films was measured at a frequency of 87 GHz using a cylindrical cavity made of OFHC copper (Fig. 1). The samples were mounted as one cavity end plate and fixed with a Cu-Be spring. The microwave power was transmitted to and from the cavity by circular waveguides made of silver and was coupled in and out through two small holes of equal size in the cylinder wall. The field was polarized by rectangular-to-circular waveguide adapters outside the cryostat. The cavity was evacuated through the coupling holes and the waveguides, which were vacuum sealed from the other microwave components by Kapton windows. The measurements were performed during warmup in a commercial glass cryostat. After cooling with liquid helium to 4.2 K, the thermal losses of the system are sufficient to warm it up to 150 K in 3–4 h without using a heater.

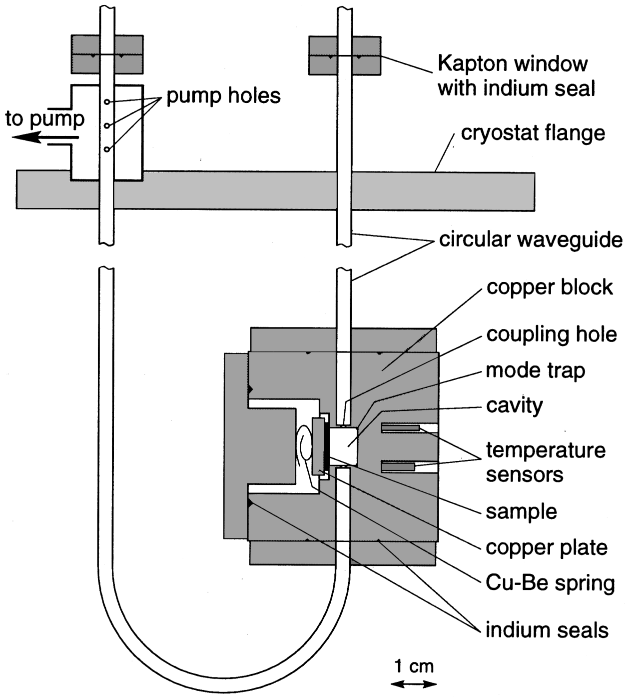

FIG. 1. Sketch of the 87 GHz copper cavity.

The rather high frequency offers a better measurement accuracy compared to similar copper cavities operating at lower frequencies, because the microwave losses in the normal conducting cavity wall increase much slower with frequency ($\sim\omega^{0.5}$) than those in the superconducting sample ($\sim\omega^2$). The dimensions of the cavity have been chosen in a way that it can be used for films of the standard size 10×10 mm^2 and excited in the TE$_{013}$ mode as well as in the TE$_{021}$ mode at frequencies near 87 GHz. The magnetic field distributions of the two modes are shown in Fig. 2. For both of them, the field at the sample surface induces circulating currents parallel to the ab planes of the YBCO films. There are no contributions to the microwave losses from currents along the c direction of the YBCO material and no peaks in the field distribution due to demagnetization effects, as they may occur in cavity perturbation measurements on single crystals, where the crystals are placed inside a cavity.[19,20,27,76,64] According to the field distributions of both modes (see Fig. 2), there should be no currents flowing over the joint between cavity and sample. However, it turned out to be very important to have smooth, plain, and clean surfaces at the joint to avoid parasitic losses.

The microwave coupling holes are positioned in the middle of the cylinder wall where the z component of the magnetic field of both TE modes has a maximum (see Figs. 1 and 2). Because the microwave coupling strength gives a significant contribution to the experimental error of the sur-

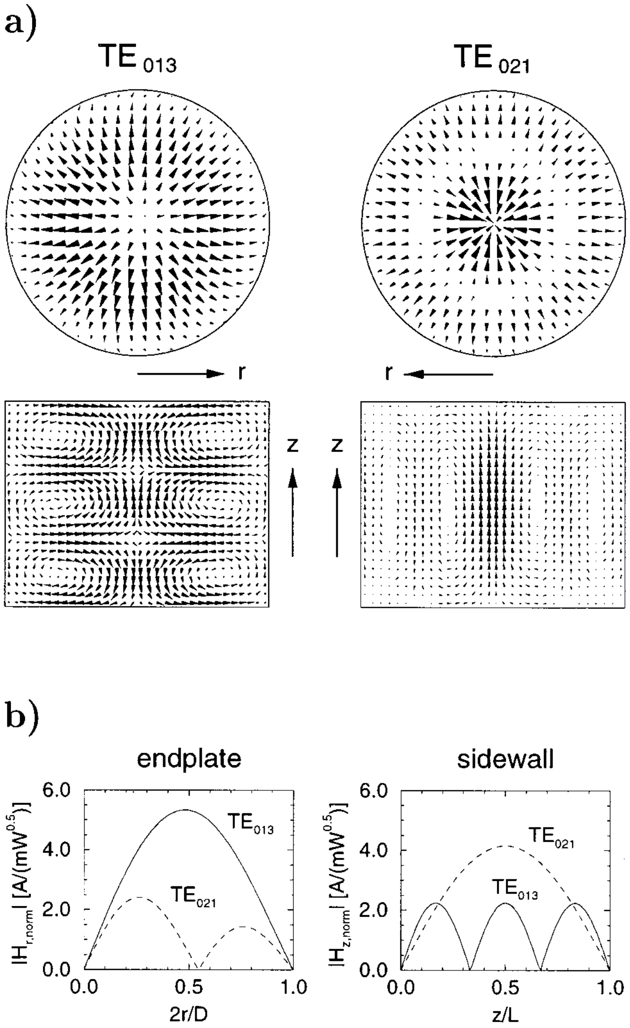

FIG. 2. (a) Images of the field distributions at the end plate and along the cross section of the cavity for the TE_{013} mode (left side) and the TE_{021} mode (right side), respectively. (b) Normalized microwave field amplitudes $|H_{r,\mathrm{norm}}|=|H_r|/\sqrt{P_0Q_0}$ along the normalized radius $2r/D$ of the cavity end plate (left side) and $|H_{z,\mathrm{norm}}|=|H_z|/\sqrt{P_0Q_0}$ along the normalized length z/L of the cavity sidewall (right side) for both modes, respectively.

face resistance (see below), the coupling holes were designed to provide a weak coupling for both modes in their specific measurement ranges. The frequencies of the corresponding TM_{113} and TM_{121} modes are shifted about 300 MHz away from those of the TE modes because of field distortions due to the coupling holes and the steplike mode trap at the bottom of the resonator. Furthermore, these modes should only be weakly excited for two reasons: First, the coupling should be very weak due to the orthogonal polarization and the vanishing of the magnetic field at the center of the coupling hole and second, the quality factors are expected to be low due to joint currents. In fact, these modes have never been observed.

Since the first version of the experimental setup was published,[1] several important changes have been made to improve the measurement accuracy and reproducibility.[77] The original cavity has been replaced by a new one with smaller coupling holes. It was fabricated by sparc erosion followed by chemical polishing to obtain smooth surfaces, especially in the joint region, and to avoid grooves that had occurred in the old cavity due to its machining. A programable sweep synthesizer combined with a frequency extender, which generates the sixth harmonic of its input frequency, is used as microwave source now. Due to the low output power of the frequency extender (~1 mW) and the weak coupling of the cavity, the maximum surface field H_s at the sample is limited to about 20 A/m. As microwave detector a sensitive bolometric powermeter (or, alternatively, a detector diode and a digital voltmeter) is used. The complete measurement process is computer controlled. The transmitted power P is measured as a function of the stepwise swept frequency f of the input signal. The resonant frequency f_r and the loaded quality factor Q_L of the cavity are determined from Lorentzian fits to these $P(f)$ data. The temperature of the cavity is measured before and after each frequency sweep and the average values are taken. These steps are repeated continuously during the warmup time of the cavity.

In order to convert f_r and Q_L into a change of penetration depth and a surface resistance of the sample we need some characteristic parameters of the two TE modes for the design values of our cavity, i.e., a diameter of $D=8.11$ mm and a length of $L=6.05$ mm: The resonance frequency is given by

$$f_{0np}=\frac{c}{2}\sqrt{\left(\frac{2x_{0n}}{\pi D}\right)^2+\left(\frac{p}{L}\right)^2} \tag{2}$$

where x_{0n} is the nth zero of the first derivative of the zeroth Bessel function. The geometric factor

$$G=2\pi\mu_0 f_{0np}\frac{\int_V H^2dV}{\int_S H^2dA} \tag{3}$$

of a resonator describes the relation between the unloaded quality factor $1/Q_0=1/Q_L-2/Q_{\mathrm{coupling}}$ and the surface resistance R_s: $1/Q_0=R_s/G$. Q_{coupling} accounts for losses due to radiation through each of the two coupling holes. If a part of the copper resonator is replaced by a sample of a different material, the relation is modified to

$$\frac{1}{Q_0}=\frac{R_{s,\mathrm{sample}}}{G_{\mathrm{sample}}}+R_{s,\mathrm{Cu}}\left(\frac{1}{G}-\frac{1}{G_{\mathrm{sample}}}\right). \tag{4}$$

Here, G_{sample} is the partial geometric factor in which the surface integral Eq. (3) extends only over that part of the cavity surface covered by the sample. The ratio G/G_{sample} is thus a measure for the contribution of the sample to the total microwave losses in the cavity walls.

The corresponding relation between the change in resonance frequency and the change in penetration depth reads

$$\Delta f_r=-\frac{\pi\mu_0 f_{0np}^2}{G_{\mathrm{sample}}}\left[\Delta\lambda_{\mathrm{sample}}+\Delta\lambda_{\mathrm{Cu}}\left(\frac{G_{\mathrm{sample}}}{G}-1\right)\right]. \tag{5}$$

It follows from this equation that the prefactor can be interpreted as derivative of the resonant frequency with respect to the cavity length L: $-\pi\mu_0 f_{0np}^2/G_{\mathrm{sample}}=\partial f/\partial L$. The geometric parameters f_{0np}, G, G_{sample}, and $\partial f/\partial L$ have been calculated analytically and are listed in Table I. With the help of these parameters we obtain the surface resistance of the sample from the measured Q_L according to

TABLE I. Characteristic parameters of the TE_{013} and the TE_{021} mode of the 87 GHz copper cavity.

Mode	f_r(4.2 K) [GHz]	G [Ω]	G_{sample} [Ω]	G/G_{sample} [%]	$\partial f/\partial L$ [kHz/nm]
TE_{013}	86.85	1115	2842	39.2	−10.47
TE_{021}	86.31	1343	24928	5.4	−1.17

$$R_{s,\mathrm{sample}}(T)=G_{\mathrm{sample}}\left(\frac{1}{Q_L(T)}-\frac{2}{Q_{\mathrm{coupling}}}\right) -R_{s,\mathrm{Cu}}(T)\left(\frac{G_{\mathrm{sample}}}{G}-1\right), \tag{6}$$

while changes in penetration depth $\Delta\lambda_{\mathrm{sample}}$ of the sample can be derived from the changes of f_r:

$$\Delta\lambda_{\mathrm{sample}}(T)=\left(\frac{\partial f}{\partial L}\right)^{-1}[\Delta f_r(T)-\Delta f_{\mathrm{cavity}}(T)]+\Delta\lambda_{\mathrm{Cu}}(T). \tag{7}$$

$R_{s,\mathrm{Cu}}$ and $\Delta f_{\mathrm{cavity}}$ are determined from calibration measurements with copper samples. Subtracting $\Delta f_{\mathrm{cavity}}$ removes the effect of thermal expansion of the cavity (which amounts to $\Delta L\approx 3\mu$m between 4.2 and 100 K) on the resonant frequency. Frequency shifts and hence penetration depth changes are measured relative to their values at the lowest attainable temperature, viz. 4.2 K. $\Delta\lambda_{\mathrm{Cu}}$ is calculated from the measured $R_{s,\mathrm{Cu}}$ data with the $\lambda(R_s)$ relation for the anomalous skin effect,[78] because it cannot be determined directly. However, the influence of this correction is small, since $\Delta\lambda_{\mathrm{Cu}}$ from 4.2 to 90 K amounts to only a few percent of $\Delta\lambda_{\mathrm{sample}}$ for YBCO samples. It is not possible to derive absolute values for the penetration depth, because the dimensions of the cavity cannot be determined with sufficient accuracy for obvious reasons. Furthermore, the absolute values of f_r may slightly vary between different measurements due to, e.g., the exact sample position or changes of the air pressure, but the shape of the temperature dependence of f_r, which is important for the determination of $\Delta\lambda_{\mathrm{sample}}(T)$, is reproducible within certain error limits (see below).

Because of the high ratio G/G_{sample} and the rather large $\partial f/\partial L$ (see Table I), the TE_{013} mode offers a high measurement sensitivity for the surface resistance as well as for the penetration depth changes of the sample. Due to this high sensitivity and the weak coupling, i.e., a high $Q_{\mathrm{coupling}}\approx 2\times 10^6$, this mode can only be used for $R_{s,\mathrm{sample}}$ below about 0.3 Ω, i.e., in the superconducting state. At higher $R_{s,\mathrm{sample}}$ values the transmitted microwave power becomes too low for the quality factor of the cavity to be determined. However, in that $R_{s,\mathrm{sample}}$ regime the TE_{021} mode can be used. It is much less sensitive due to its lower G/G_{sample} and provides a lower $Q_{\mathrm{coupling}}\approx 3\times 10^5$, thus allowing measurements even in the normal conducting regime, but with reduced accuracy.

The sensitivity for changes of $R_{s,\mathrm{sample}}$ and thus for the shape of the $R_{s,\mathrm{sample}}(T)$ curves depends only on the statistical error in the determination of Q_L, which is between $\pm 0.5\%$ (for high Q_L) and $\pm 1\%$ (for low Q_L). The resulting resolution for $R_{s,\mathrm{sample}}$ measurements is in the TE_{013} mode about ± 0.3 mΩ for high $Q_L>60000$, corresponding to $R_{s,\mathrm{sample}}<5$ mΩ, and about ± 4mΩ for the lowest measurable $Q_L\approx 8000$, corresponding to $R_{s,\mathrm{sample}}\approx 300$ mΩ. For the TE_{021} mode it varies between at best ± 5 mΩ for $R_{s,\mathrm{sample}}\approx 300$ mΩ and about ± 125 mΩ for the upper measurement limit of $R_{s,\mathrm{sample}}\approx 10$ Ω. However, the absolute accuracy of $R_{s,\mathrm{sample}}$, which is important for comparisons to theory and to results of other measurement techniques, depends additionally on the systematic errors of Q_{coupling} and of $R_{s,\mathrm{Cu}}$. Usually, Q_{coupling} is determined from the incident, the reflected, and the transmitted microwave power at the cavity. But due to significant contribution of standing waves to the measured millimeter wave signals, the accuracy of this method is limited to about $\pm 10\%$. Therefore, calibration measurements with niobium films and copper samples have been performed. The resulting absolute accuracy of $R_{s,\mathrm{sample}}$ mainly depends on the reproducibility (after reassembly of the samples) of these measurements. It was found to be better than ± 1mΩ for the TE_{013} mode at high Q_L and temperatures below 25 K, where $R_{s,\mathrm{Cu}}$ is nearly constant. The calibration measurements have also proved that the parasitic losses at the joint between sample and cavity wall can be kept sufficiently small. The resolution and the absolute error of $R_{s,\mathrm{sample}}$ are summarized for both modes and different $R_{s,\mathrm{sample}}$ ranges in Table II.

For the TE_{013} mode, changes of the resonant frequency as small as ~ 2 kHz can be resolved (at high Q_L and constant pressure in the cryostat and the cavity), which would correspond to penetration depth changes of about 0.2 nm. But the accuracy of $\Delta\lambda_{\mathrm{sample}}$ depends mainly on the reproducibility of $f_r(T)$ and $f_{\mathrm{cavity}}(T)$. It is therefore not limited by the accuracy of the frequency measurement, but by possible small variations of the resonant frequency itself due to other effects, such as changes of the pressure in the cavity or the cryostat. The resulting absolute errors of $\Delta\lambda_{\mathrm{sample}}$ are also summarized in Table II. The best relative accuracy is ob-

TABLE II. Resolution of $R_{s,\mathrm{sample}}$ and absolute errors of $R_{s,\mathrm{sample}}$ and $\Delta\lambda_{\mathrm{sample}}$ for different ranges of $R_{s,\mathrm{sample}}$.

$R_{s,\mathrm{sample}}$ [mΩ]	Resolution of $R_{s,\mathrm{sample}}$ [mΩ]	Abs. error of $R_{s,\mathrm{sample}}$ [mΩ]	Abs. error of $\Delta\lambda_{\mathrm{sample}}$ [nm]	Mode
<50	±0.3 for $T<25$ K	±1 for $T<25$ K	±0.7 for $T<25$ K	TE_{013}
	±0.3–1 for $T>25$ K	±1.5–2 for $T>25$ K	±2−5 for 25 K$<T<$55 K	
50–300	±1–4	±2–6	±5–8 for $T>55$ K	
300–10 000	±5–125	±40–150		TE_{021}

tained at temperatures below ~25 K, where the thermal expansion is small, and above ~55 K, where the penetration depth change of the sample is large. Because of the reduced sensitivity of the TE_{021} mode (see Table I), penetration depth changes could only be determined from data obtained with the TE_{013} mode.

Changes of the temperature can be detected with an accuracy of about ±0.1 K, but the absolute error of the temperature measurements can be as high as 0.5 K due to the characteristics of the temperature sensors. The T_c values of the YBCO films can be estimated from the drop in the measured surface resistance. For both samples, they have been found to be in good agreement with the results of the inductive measurements.

C. Surface impedance analysis

The measured $R_{s,\mathrm{sample}}$ and $\Delta\lambda_{\mathrm{sample}}$ data are only identical to the ''real'' material specific surface resistance and penetration depth change values of the sample, if the film thickness is large compared to the field penetration depth. As the given film thickness of $d=350$ nm is of the same order of magnitude as the penetration depth values of YBCO, the measured effective data are higher than the material specific values.[79] This is mainly due to changes of the current distribution in the film, which depend on the ratio d/λ. If the thicknesses and impedances of the film, the substrate, and the copper plate are known, the effective surface impedance of this sandwich structure can be calculated by a sequence of impedance transformations. For the comparison with theory, which provides the local dielectric function $\varepsilon(\omega)=\varepsilon_0[1+(i/\varepsilon_0\omega)\sigma(\omega)]$ for homogeneous systems, one needs the material specific surface impedance values of the film, i.e., the thickness-corrected surface resistance R_s and penetration depth λ. Even though the quasiparticle mean free paths at low temperatures may exceed the penetration depth, only the local limit of the constitutive relations of electrodynamics needs to be considered in the case of $\hat{c}$-axis oriented HTC films because of the high degree of anisotropy characteristic of these materials.[80,81] The surface impedance Eq. (1) is thus related to the complex conductivity $\sigma(\omega)=\sigma_1(\omega)+i\sigma_2(\omega)$ according to

$$R_s(\omega)-i\omega\mu_0\lambda(\omega)=\sqrt{\frac{\omega\mu_0}{i\sigma_1(\omega)-\sigma_2(\omega)}} \tag{8}$$

since the displacement current is negligible at the frequencies of interest.

R_s and λ can be determined from the measured effective data by inverting the impedance transformation process. Analytical expressions for a first-order approximation of the impedance transformations are given in Ref. 79. For a more precise analysis, a numerical iteration procedure was used here for the inversion of the impedance transformations, which requires absolute values for both $R_{s,\mathrm{sample}}$ and $X_{s,\mathrm{sample}}$. In the superconducting state $X_s=\omega\mu_0\lambda$ is determined from the measured penetration depth data of the TE_{013} mode. Because the measurements provide only information about temperature dependent changes and not about absolute values of $\lambda_{\mathrm{sample}}$, an offset for the $\Delta\lambda_{\mathrm{sample}}(T)$ curve has to be suitably chosen to give reasonable values for the thickness corrected $\lambda(0)$. In the normal state the relation $X_s=R_s$ is used, consistent only with the normal skin effect regime $\sigma=\sigma_1$, because no independent penetration depth data are available from the measurements with the TE_{021} mode as mentioned above. The normal-state resistivity $\rho=1/\sigma_1$ can then be calculated from R_s according to $\rho=(2R_s^2)/(\omega\mu_0)$. Its accuracy is limited, apart from the error of $R_{s,\mathrm{sample}}$, by the uncertainty of the film thickness to about ±10%. In the superconducting regime the errors due to uncertainties of the film thickness values (about ±10%) can be neglected compared to the errors of $R_{s,\mathrm{sample}}$ and $\Delta\lambda_{\mathrm{sample}}$ for the present samples. However, a problem occurs in the region near T_c, where the TE_{013} mode can no longer be used, because $R_{s,\mathrm{sample}}$ is too high. In this temperature regime the conductivity is complex due to superconducting fluctuations or sample inhomogeneity so that our method of obtaining the penetration depth or X_s from the measurements with the TE_{021} mode, which is based on the normal skin effect formula, fails. This failure shows up very clearly in the inset of Fig. 7(a) as well as in Fig. 6, were all available data have been included in order to demonstrate the limits of the normal skin effect regime.

According to Eqs. (1) and (8) the real part σ_1 of the complex conductivity can be obtained from R_s and X_s:[3]

$$\sigma_1=2\omega\mu_0\frac{R_sX_s}{(R_s^2+X_s^2)^2}. \tag{9}$$

In the case of the normal skin effect ($R_s=X_s$), this reduces to $1/\rho$. In the superconducting regime with $R_s\ll X_s$, σ_1 can be approximated as

$$\sigma_1=(2R_s)/(\omega^2\mu_0^2\lambda^3). \tag{10}$$

Therefore, σ_1 is very sensitive to small changes of λ and thus also to its errors. For the same reason as for the thickness correction, it is not possible to derive reliable values for σ_1 close to T_c.

The surface resistance values obtained for the samples A and B (see Figs. 8 and 13) are typical for high-quality films, which have been optimized for low microwave losses, and can be reproducibly obtained by both deposition techniques. In view of the similarity in doping levels, values for $\lambda(0)$ of 140 and 160 nm have been used for the thickness correction calculations. These values are in good agreement with results for YBCO films and single crystals from techniques that allow an absolute determination of the penetration depth.[30–35] In the case of Sample B, choosing $\lambda(0)=160$ nm improves the agreement between experimental data and theoretical calculations.

III. THEORETICAL BACKGROUND

A. Generalities

The local in-plane conductivity $\sigma(\omega)$ required in the surface impedance analysis (cf. Sec. II C) is calculated using linear response theory. Many-body effects are taken into account in the quasiclassical approximation in which it is assumed that the main contributions to self-energy corrections and correlation functions come from quasiparticle states near the Fermi surface. Due to their layered structure, Fermi surfaces of HTC materials are nearly cylindrical. Concentrating on the contribution from the CuO_2 planes which, neglecting the small orthorhombic distortion, have quadratic symmetry, we can replace $v_x^2(\boldsymbol{k}_F)$ by $\frac{1}{2}[v_x^2(\boldsymbol{k}_F)+v_y^2(\boldsymbol{k}_F)]=\frac{1}{2}v^2(\boldsymbol{k}_F)$ in the current-current correlation function. Effects due to the variation of the Fermi velocity with $\boldsymbol{k}_F$ have been studied by some of the present authors.[61] The changes in the surface impedance resulting from different physically plausible assumptions with respect to $v^2(\boldsymbol{k}_F)$ were found to be fairly small and purely quantitative. The momentum dependence of scattering events can be expected to introduce similar changes. Here we shall neglect these effects and replace the Fermi velocity and the density of states per spin at the Fermi level by some averaged values v_F and $N(0)$. These are combined into a single parameter, the plasma wavelength λ_p, according to

$$\frac{1}{\mu_0\lambda_p^2}=e^2N(0)v_F^2. \tag{11}$$

If the Fermi surface actually has a circular cross section (free electrons in two dimensions) one has for the density of states per spin $N(0)=m/2\pi$ and for the particle density $n=m^2v_F^2/2\pi$ so that our definition of λ_p reduces to the usual one:

$$\lambda_p=\frac{c}{\omega_{pl}}=\sqrt{\frac{m}{ne^2\mu_0}}. \tag{12}$$

λ_p is one of the important parameters in our theory. With these simplifications the conductivity for a homogeneous superconductor is calculated from[21,36,82–84,61]

$$\begin{aligned}\sigma(\omega)=\frac{1}{\mu_0\lambda_p^2}\frac{1}{2\omega}\int_{-\omega/2}^{+\infty}d\Omega\Bigg\{&\tanh\frac{\Omega+\omega}{2T}2i\,\mathrm{Im}\\&\times\langle M(\boldsymbol{k}_F;\Omega_++\omega,\Omega_+)\rangle-\left[\tanh\frac{\Omega+\omega}{2T}-\tanh\frac{\Omega}{2T}\right]\\&\times\langle M(\boldsymbol{k}_F;\Omega_++\omega,\Omega_+)\rangle+\left[\tanh\frac{\Omega+\omega}{2T}-\tanh\frac{\Omega}{2T}\right]\\&\times\langle M(\boldsymbol{k}_F;\Omega_++\omega,\Omega_-)\rangle\Bigg\},\end{aligned} \tag{13}$$

where $+(-)$ indicates a positive (negative) infinitesimal imaginary part. The brackets indicate an average over the Fermi surface. It is only through the superconducting pair state that we still have a dependence on the Fermi wave vector. In order to obtain such a pair state a momentum-dependent interaction is required. When the contribution of this interaction to the conductivity is considered within the framework of a strong-coupling theory, vertex corrections would have to be taken into account.[43] We shall use a weak-coupling theory so that pairing interaction and scattering processes are not treated on the same footing. This allows us to neglect the momentum dependence of scattering events so that for singlet pairing vertex corrections vanish.[36] The quantity M is then given in terms of an integral with respect to energy over the trace of the product of two single-particle Green's functions

$$\begin{aligned}M(\boldsymbol{k}_F;\Omega_\pm+\omega,\Omega_\pm)=\frac{1}{2\pi}\int_{-\infty}^{+\infty}d\varepsilon\,\mathrm{Tr}[&\hat{G}(\varepsilon,\boldsymbol{k}_F,\Omega_\pm+\omega)\\&\times\hat{G}(\varepsilon,\boldsymbol{k}_F,\Omega_\pm)]\end{aligned} \tag{14}$$

with

$$\hat{G}(\varepsilon,\boldsymbol{k}_F,\Omega_\pm)=-\frac{\Omega Z\hat{\tau}_0+(\varepsilon+\chi)\hat{\tau}_3+\phi\hat{\tau}_1}{-(\Omega_\pm Z)^2+(\varepsilon+\chi)^2+\phi^2}. \tag{15}$$

The $\hat{\tau}_i$'s are Pauli matrices. For the self-energy corrections Z, χ, ϕ the values at the Fermi level are inserted so that the energy integral is easily performed:

$$\begin{aligned}&M(\boldsymbol{k}_F;\Omega_\pm+\omega,\Omega_\pm)\\&=\left(1+\frac{(\Omega+\omega)Z(\Omega_\pm+\omega)\Omega Z(\Omega_\pm)+\phi(\Omega_\pm+\omega)\phi(\Omega_\pm)}{R(\Omega_\pm+\omega)R(\Omega_\pm)}\right)\\&\times\frac{R(\Omega_\pm)+R(\Omega_\pm+\omega)}{[R(\Omega_\pm)+R(\Omega_\pm+\omega)]^2+[\chi(\Omega_\pm)-\chi(\Omega_\pm+\omega)]^2},\end{aligned} \tag{16}$$

where

$$R(\boldsymbol{k}_F,\Omega_\pm)=\sqrt{\phi^2(\boldsymbol{k}_F,\Omega_\pm)-[\Omega Z(\boldsymbol{k}_F,\Omega_\pm)]^2}. \tag{17}$$

In the absence of scattering the real order parameter ϕ is determined from the self-consistency equation involving a sum over Matsubara frequencies $\omega_n=(2n+1)\pi T$ and a cutoff ω_c:

$$\phi(\boldsymbol{k}_F)=N(0)\pi T\sum_{\omega_n<\omega_c}\left\langle V(\boldsymbol{k}_F,\boldsymbol{k}_F')\frac{\phi(\boldsymbol{k}_F')}{\sqrt{\phi^2(\boldsymbol{k}_F')+\omega_n^2}}\right\rangle. \tag{18}$$

We shall concentrate in this paper on a d-wave order parameter of the form[21,53,85,38]

$$\phi(\boldsymbol{k}_F)=\Delta_0(T)\cos 2\varphi, \tag{19}$$

where φ specifies the orientation of the two-dimensional internal momentum $\boldsymbol{k}_F$ of the Cooper pairs. The weak-coupling pairing interaction $V(\boldsymbol{k}_F,\boldsymbol{k}_F')$ has to be suitably chosen to give the solution Eq. (19). Solving this self-consistency equation one obtains the temperature dependence of the amplitude $\Delta_0(T)$, which is found to be very similar to that of an isotropic order parameter except that $2\Delta_0(0)/k_BT_c=4.29$ rather than 3.52. In order to establish which features of the d-wave state are truly significant for the microwave response we shall include some results for the anisotropic s-wave states:

$$\phi_{as+}(\boldsymbol{k}_F)=\Delta_0(T)|\cos 2\varphi|, \tag{20a}$$

$$\phi_{as\epsilon}(\boldsymbol{k}_F)=\Delta_0(T)(\epsilon+\cos 4\varphi)\frac{1}{1+\epsilon}, \quad \epsilon\geqslant 0. \tag{20b}$$

The state Eq. (20a) has been chosen because in the clean limit it leads to the same nodal structure of the energy gap and to the same density of states as the d-wave state Eq. (19), but does not change sign.[52] The state Eq. (20b) has been included because it allows us to study the effects of sign changes.[86] $\phi_{as\epsilon=0}$ shares with Eq. (19) not only the property that the Fermi surface average vanishes. It gives, in fact, exactly the same results as Eq. (19) since $\langle f\rangle\equiv\int_0^{2\pi}f(\cos n\varphi)d\varphi$ is independent of the integer n. Another state with similar properties is the real combination of s- and d-wave states

$$\phi_{s+d}(\boldsymbol{k}_F)=\Delta_0(T)(\eta_0+\cos 2\varphi), \tag{21}$$

where η_0 is some real constant with $|\eta_0|<1$. The distribution of nodes no longer shows square symmetry so that this state can be used to describe anisotropy in the conductivity.[67]

Finite quasiparticle lifetimes are caused by elastic scattering off point defects, which is treated in the $\hat{t}$-matrix approximation, but with only s-wave scattering included. Because of this restriction to isotropic scattering there are no vertex corrections to the current-current correlation function. In the presence of isotropic elastic scattering, Eq. (18) is generalized to

$$\tilde{\phi}(\boldsymbol{k}_F,\Omega_\pm)=\phi(\boldsymbol{k}_F)+\Gamma_N^{\mathrm{el}}\frac{\langle g_1(\boldsymbol{k}_F,\Omega_\pm)\rangle}{\cos^2\delta_N-\sin^2\delta_N(\langle g_0(\boldsymbol{k}_F,\Omega_\pm)\rangle^2-\langle g_1(\boldsymbol{k}_F,\Omega_\pm)\rangle^2)}, \tag{22}$$

while the remaining self-energy corrections are to be determined from

$$\Omega Z(\Omega_\pm)=\Omega+\Gamma_N^{\mathrm{el}}\frac{\langle g_0(\boldsymbol{k}_F,\Omega_\pm)\rangle}{\cos^2\delta_N-\sin^2\delta_N(\langle g_0(\boldsymbol{k}_F,\Omega_\pm)\rangle^2-\langle g_1(\boldsymbol{k}_F,\Omega_\pm)\rangle^2)}\pm i\Gamma^{\mathrm{inel}}(T,\Omega) \tag{23}$$

and

$$\chi(\Omega_\pm)=\Gamma_N^{\mathrm{el}}\frac{\cot\delta_N}{\cos^2\delta_N-\sin^2\delta_N(\langle g_0(\boldsymbol{k}_F,\Omega_\pm)\rangle^2-\langle g_1(\boldsymbol{k}_F,\Omega_\pm)\rangle^2)}. \tag{24}$$

g_0 and g_1 are the energy-integrated normal and anomalous Green's functions

$$g_0(\boldsymbol{k}_F,\Omega_\pm)=\frac{\Omega Z(\Omega_\pm)}{\sqrt{\tilde{\phi}^2(\boldsymbol{k}_F,\Omega_\pm)-[\Omega Z(\Omega_\pm)]^2}}, \tag{25}$$

$$g_1(\boldsymbol{k}_F,\Omega_\pm)=\frac{\tilde{\phi}(\boldsymbol{k}_F,\Omega_\pm)}{\sqrt{\tilde{\phi}^2(\boldsymbol{k}_F,\Omega_\pm)-[\Omega Z(\Omega_\pm)]^2}}. \tag{26}$$

Here,

$$\Gamma_N^{\mathrm{el}}=n_{\mathrm{imp}}\frac{\pi N(0)v^2}{1+[\pi N(0)v]^2} = \frac{n_{\mathrm{imp}}}{\pi N(0)}\sin^2\delta_N \tag{27}$$

is the elastic state scattering rate in the normal state and $\delta_N=\tan^{-1}[\pi N(0)v]$ is the scattering phase shift. The self-energy χ reduces to a real constant, which can be absorbed in the chemical potential, when the scattering is weak ($\delta_N\rightarrow 0$, Born approximation) and it vanishes for strong scattering ($\delta_N=\pi/2$, unitary limit). For arbitrary phase shifts it is important to keep χ (Ref. 87) (see Fig. 10). Writing in Eq. (22) simply $\phi(\boldsymbol{k}_F)$ for the right-hand side of Eq. (18) means that we are neglecting the effect of elastic scattering on T_c and on the temperature dependence of the order-parameter amplitude $\Delta_0(T)$. This is justified because we only need to consider very small values of Γ_N^{el}. In Eq. (23) a scattering rate arising from inelastic scattering processes, to be discussed below, has been included. It would be inconsistent with our weak-coupling approximation to include this scattering explicitly in Eq. (22).[88]

For an isotropic order parameter one has $\langle g_0\rangle^2-\langle g_1\rangle^2=-1$ so that the corrections to Ω and ϕ are independent of δ_N and the usual BCS results are easily derived. The other extreme is an order parameter whose Fermi surface average vanishes. In such a case $\phi(\boldsymbol{k}_F)$ remains unchanged to lowest order with respect to elastic s-wave scattering, while the correction to Ω becomes very large in the unitarity limit $\delta_N=\pi/2$ resulting in strong scattering effects. Order parameters with some finite Fermi surface average less than $\Delta_0(0)$ interpolate between these extremes which leads to a much reduced influence of the scattering phase shift.[89]

For pure s-wave scattering we can put $\langle g_1\rangle\equiv 0$ provided it vanishes in the clean limit, as is the case for the d-wave state Eq. (19) as well as for the state $\phi_{as\epsilon=0}$, Eq. (20b). Then $\tilde{\phi}=\phi$ is independent of frequency and Eq. (16) can be simplified to

$$M(\boldsymbol{k}_F;\Omega_\pm+\omega,\Omega_\pm)=\left(\frac{g_0(\boldsymbol{k}_F,\Omega_\pm+\omega)-g_0(\boldsymbol{k}_F,\Omega_\pm)}{(\Omega+\omega)Z(\Omega_\pm+\omega)-\Omega Z(\Omega_\pm)}\right)\frac{[R(\Omega_\pm)+R(\Omega_\pm+\omega)]^2}{[R(\Omega_\pm)+R(\Omega_\pm+\omega)]^2+[\chi(\Omega_\pm)-\chi(\Omega_\pm+\omega)]^2}. \tag{28}$$

This is further simplified in the two limiting cases $\delta_N=0$ and $\delta_N=\pi/2$ where the factor involving χ reduces to 1. The resulting equation has been given by Klemm *et al.* [Ref. 36, Eq. (46a)] and Hirschfeld *et al.* [Ref. 21, Eq. (15)]. These limiting cases have been studied most frequently because for many unconventional pair states and sufficiently simple Fermi surfaces the Fermi surface averages can be evaluated analytically.

Γ_N^{el} depends on the concentration of scattering centers n_{imp}, the density of states at the Fermi level $N(0)$, and the screened scattering potential v. None of these quantities are expected to vary much with temperature. In the superconducting state even purely elastic scattering leads, according to Eq. (23), to a temperature-dependent scattering rate because the phase space available for elastic scattering changes with the superconducting order parameter. This effect is routinely taken into account and does not suffice to explain the temperature dependence of the surface impedance. With transition temperatures around 100 K it is not surprising that inelastic-scattering processes should make a significant contribution to the quasiparticle lifetime over much of the temperature range below T_c. We shall assume that the various contributions to the self-energy do not interfere, i.e., we assume Matthiessen's rule be applicable.[90] There are cases in which this assumption is unjustified[91] but with regard to high-T_c superconductors there seems to be no reason to question its validity.

In HTC materials, a very likely source for a temperature-dependent self-energy correction contributing to Z would be spin fluctuation exchange.[21,92,60] This could be taken into account purely phenomenologically by including some function $i\Gamma^{\mathrm{inel}}(T)$ on the right-hand side of Eq. (23). One would expect that for each experimental frequency a different function would have to be used.

It is, of course, possible to calculate the self-energy due to spin fluctuations exchange, but such calculations are rather involved.[92,60] We shall employ the approximation introduced by Ruvalds *et al.*[60] in view of the nesting properties of the Fermi surfaces of HTC materials. The real part of the self-energy is neglected while the imaginary part is found to be given by

$$\Gamma_{\mathrm{NFL}}^{\mathrm{inel}}(T,\Omega)=g^2\int_{-\infty}^{+\infty}d\omega\frac{1}{N(0)}\chi_{SF}''(\boldsymbol{Q};\omega)\times\frac{1}{2}\left[\coth\frac{\omega}{2T}-\tanh\frac{\omega-\Omega}{2T}\right]\tilde{N}(\Omega-\omega). \tag{29}$$

$g=N(0)U$ with U the Coulomb matrix element (the "Hubbard U") is treated as an adjustable parameter. The variation of the scattering rate with momentum[92] is neglected here. The imaginary part of the spin susceptibility χ_{SF}'' is taken at the nesting vector $\boldsymbol{Q}$ rather than being integrated with respect to momentum. The quantity $\tilde{N}$ is the normalized density of states which has been studied extensively for a variety of unconventional pair states with particular emphasis on the effects arising from elastic impurity scattering.[50,51,93–98] For the d-wave order parameter Eq. (19) and with scattering neglected $\tilde{N}$ can be calculated analytically if a cylindrical Fermi surface with circular cross section is assumed:

$$\tilde{N}_0(\Omega-\omega)=\mathrm{Im}\left\langle\frac{(\Omega-\omega)}{\sqrt{\phi^2(\boldsymbol{k}_F)-(\Omega-\omega)^2}}\right\rangle=\begin{cases}\dfrac{2}{\pi}\dfrac{|\Omega-\omega|}{\Delta_0}K\left(\dfrac{|\Omega-\omega|}{\Delta_0}\right) & |\Omega-\omega|<\Delta_0,\\[2ex] \dfrac{2}{\pi}K\left(\dfrac{\Delta_0}{|\Omega-\omega|}\right) & |\Omega-\omega|>\Delta_0.\end{cases} \tag{30}$$

When only the simplest spin fluctuation diagram is included, $\chi_{SF}''(\boldsymbol{Q};\omega)$ can also be obtained analytically using the same simplifying assumptions:[60]

$$\frac{1}{N(0)}\chi_{SF}''(\boldsymbol{Q};\omega)=\frac{\pi}{2}\tanh\frac{\omega}{4T}\tilde{N}\left(\frac{|\omega|}{2}\right). \tag{31}$$

As we shall see, keeping the frequency dependence of $\Gamma_{\mathrm{NFL}}^{\mathrm{inel}}(T,\Omega)$ leads to results significantly different from those obtained with a purely temperature dependent scattering rate. Since the frequency dependence of $\Gamma_{\mathrm{NFL}}^{\mathrm{inel}}$ has to be integrated over in Eq. (13) it is essential to simplify the calculation of the spin fluctuation exchange as much as possible. This is the reason why the calculation of the density of states Eq. (30) is not done self-consistently.

At zero frequency the integration in Eq. (29) is restricted to $|\omega|\leqslant 2T$ so that at low temperatures the elliptic integral K appearing in Eq. (30) can be replaced by $\pi/2$, yielding a linear frequency dependence of the density of states. This, in turn, leads to a cubic temperature dependence for the scattering rate,[92] if the order-parameter amplitude Δ_0 is replaced by its zero-temperature limit:

$$\Gamma_{\mathrm{NFL}}^{\mathrm{inel}}(T,0)=3.68g^2\left(\frac{T_c}{\Delta_0(0)}\right)^2\left(\frac{T}{T_c}\right)^3T_c. \tag{32}$$

At finite frequencies, scattering of quasiparticles involving emission of spin fluctuations is possible at all temperatures, including $T=0$. At small frequencies $\Omega\ll\Delta_0(0)$ one finds with the above approximations for the density of states the following zero-temperature scattering rate:

$$\Gamma_{\mathrm{NFL}}^{\mathrm{inel}}(0,\Omega)=g^2\frac{\pi}{24}\left(\frac{T_c}{\Delta_0(0)}\right)^2\left(\frac{\Omega}{T_c}\right)^3T_c. \tag{33}$$

In the normal state, $\tilde{N}(\omega)=1$ so that $\Gamma_{\mathrm{NFL}}^{\mathrm{inel}}(T,\Omega)$ Eq. (29) has the functional form $TF(\Omega/T)$. In view of Eq. (38) below this gives $\sigma(T,\omega)\propto T^{-1}$ if the external frequency is small compared to the temperature and the scattering rate. This explanation of the widely observed linear temperature dependence of the resistivity was one of the early successes of the nested Fermi-liquid (NFL) model.[60]

B. Limiting cases and approximations

Several authors have studied the zero frequency penetration depth for this d-wave model.[99–102] A range of low-temperature, low-frequency approximations to the real part of the conductivity can also be found in the literature.[21] In particular, for $T=0$ and $\omega=0$ the real part of the conductivity has been predicted to attain a universal value[103,21]

$$\sigma_{00}=\frac{1}{\mu_0\lambda_p^2\pi\Delta_0(0)}, \tag{34}$$

only weakly dependent on the elastic scattering rate and the phase shift through $\Delta_0(0)$.[98] With $\lim_{\Omega\to 0}\Omega Z(\Omega_\pm)\equiv\pm i\gamma$ we can easily obtain this result from Eqs. (13) and (28), where the correction factor can be omitted since χ Eq. (24) is real:

$$\begin{aligned}\sigma_{00}&\equiv\lim_{\omega\to 0}\lim_{T\to 0}\mathrm{Re}\,\sigma(\omega,T)\\&=\frac{1}{2\mu_0\lambda_p^2}\lim_{\Omega\to 0}\{\mathrm{Re}\langle M(\boldsymbol{k}_F;\Omega_+,\Omega_-)\rangle\\&\quad-\mathrm{Re}\langle M(\boldsymbol{k}_F;\Omega_+,\Omega_+)\rangle\}\\&=\frac{1}{2\mu_0\lambda_p^2}\left\{\frac{1}{\gamma}\mathrm{Im}\langle g_0\rangle-\frac{d}{d\gamma}\mathrm{Im}\langle g_0\rangle\right\}.\end{aligned} \tag{35}$$

As in the case of the nested Fermi-liquid model, $\langle g_0\rangle$, which is now purely imaginary, can be calculated analytically:

$$\mathrm{Im}\langle g_0\rangle=\frac{2}{\pi}\frac{\gamma}{\sqrt{\Delta_0^2(0)+\gamma^2}}K\left(\frac{\Delta_0(0)}{\sqrt{\Delta_0^2(0)+\gamma^2}}\right). \tag{36}$$

The desired result follows immediately if $\gamma\ll\Delta_0(0)$ is assumed. Hence, only scattering rates which have a negligible effect on the transition temperature and on the order-parameter amplitude are compatible with the universal conductivity.

While the limit Eq. (34) is undoubtedly correct, it seems to be of little practical consequence for experiments performed at finite frequencies unless the unitary limit applies. For Eq. (34) to be a valid approximation at finite frequencies, $\gamma\gg\omega$ has to be fulfilled. γ, however, varies rapidly with the phase shift, becoming exponentially small for $\delta_N=0$:[21,101,98]

$$\gamma=4\Delta_0(0)\exp\left(-\frac{\pi\Delta_0(0)}{2\Gamma_N^{\mathrm{el}}}\right),\quad\text{for }\Gamma_N^{\mathrm{el}}\ll\Delta_0(0),\quad\delta_N=0,$$

$$\begin{aligned}\gamma&=\sqrt{\pi\Gamma_N^{\mathrm{el}}\Delta_0(0)}\left[2\ln\frac{4\Delta_0(0)}{\gamma}\right]^{-1/2}\\&\approx\sqrt{\pi\Gamma_N^{\mathrm{el}}\Delta_0(0)}\left[\ln\frac{32\Delta_0(0)}{\pi\Gamma_N^{\mathrm{el}}}\right]^{-1/2}\\&\qquad\text{for }\Gamma_N^{\mathrm{el}}\ll\Delta_0(0),\quad\delta_N=\frac{\pi}{2}.\end{aligned} \tag{37}$$

In the next section we shall, therefore, compare experimental results obtained at the frequency $f=87$ GHz, $\hbar\omega=0.36$ meV, with the full theory as outlined in the previous section. It is, nonetheless, useful to consider some limiting cases and approximations in order to elucidate the role of the parameters in the theory and to highlight the physical origin of certain perhaps somewhat surprising features of the data. The emphasis will be on effects due to inelastic scattering.

We begin with the normal state where we have $g_0(\Omega_\pm)=\pm i$ so that Eq. (28) is simplified quite dramatically and Eq. (13) reduces to

$$\begin{aligned}\sigma_N(\omega)&=\frac{1}{\mu_0\lambda_p^2}\int_{-\omega/2}^{+\infty}d\Omega\\&\times\frac{1/\omega[\tanh(\Omega+\omega)/2T-\tanh\Omega/2T]}{-i\omega+2\Gamma_N^{\mathrm{el}}+\Gamma^{\mathrm{inel}}(T,\Omega+\omega)+\Gamma^{\mathrm{inel}}(T,\Omega)}.\end{aligned} \tag{38}$$

Further simplification is possible only if the scattering rates are frequency independent:

$$\sigma_N(\omega)=\frac{1}{\mu_0\lambda_p^2[2\Gamma_N^{\mathrm{el}}+2\Gamma^{\mathrm{inel}}(T)-i\omega]}. \tag{39}$$

A generalization of this Drude form of the conductivity to the superconducting state can be derived from Eq. (13) if we keep both frequency and temperature finite such that $\omega\ll 2T$. Neglecting the second term in Eq. (13) as well as the self-energy contribution χ Eq. (24) we have

$$\begin{aligned}\sigma(\omega)=\frac{i}{\mu_0\lambda_p^2\omega}\Bigg\{&\mathrm{Im}\int_0^{\infty}d\Omega\tanh\frac{\Omega}{2T}\frac{d}{d\Omega}\langle g_0(\boldsymbol{k}_F,\Omega_+)\rangle\\&\times\left(\frac{d\tilde{\Omega}}{d\Omega}\right)^{-1}+\omega\int_0^{\infty}d\Omega\frac{d}{d\Omega}\tanh\frac{\Omega}{2T}\\&\times\frac{\mathrm{Im}\langle g_0(\boldsymbol{k}_F,\Omega_+)\rangle}{\omega+2i\Gamma(\Omega_+)}\Bigg\}\end{aligned} \tag{40}$$

with $\tilde{\Omega}=\Omega Z(\Omega_+)\approx\Omega+i\Gamma(T,\Omega_+)$ Eq. (23). If the frequency dependence of the self-energy corrections is neglected, i.e., if $d\tilde{\Omega}/d\Omega=1$, we arrive at the two-fluid model used by several authors[19,104–106]

$$\sigma_{\text{two-fluid}}(\omega)=\frac{1}{\mu_0\lambda_p^2}\left\{\frac{1}{2\Gamma(T)-i\omega}\rho_n+\frac{i}{\omega}(1-\rho_n)\right\} \tag{41}$$

with

$$\rho_n=\int_0^{\infty}d\Omega\frac{d}{d\Omega}\tanh\frac{\Omega}{2T}\tilde{N}(\Omega). \tag{42}$$

$\tilde{N}(\Omega)=\mathrm{Im}\,\langle g_0(\boldsymbol{k}_F,\Omega_+)\rangle$ is the normalized density of states including the effects of scattering. Using the clean limit expression Eq. (30) we find at low temperatures the well-known linear T dependence

$$\rho_n=2\ln 2\frac{T}{\Delta_0(T)}. \tag{43}$$

If $\omega\ll 2\Gamma(T)$ and $\rho_n\ll 1$, then $\sigma(\omega)\approx i/\omega\mu_0\lambda_p^2(1-\rho_n)$ and from Eq. (8) we have

$$1-\rho_n=\frac{\lambda_p^2}{\lambda^2(T)}, \tag{44}$$

which is usually interpreted as superfluid density. If $\omega\gg 2\Gamma(T)$, then $\sigma(\omega)\approx i/\omega\mu_0\lambda_p^2$ and hence $\lambda_p=\lambda(T,\omega)$ independent of ρ_n. This corresponds to the relaxation regime[107] of a normal conductor. We thus expect $\lambda(T,\omega)$ to approach its limiting value very rapidly when $\Gamma(T)$ drops below ω.

For $\omega\rightarrow 0$, Eq. (41) does not reduce to the universal conductivity Eq. (34) because we neglected the second term in Eq. (13), which is small for most frequencies and temperatures. Note, that in this derivation of the two-fluid model it is essential that we are considering unconventional pairing $\langle\phi(\boldsymbol{k}_F)\rangle=0$ and momentum-independent scattering so that there are no self-energy corrections to the order parameter and M Eq. (16) can be reduced to Eq. (28). Furthermore, the density of states has to be sufficiently benign so that the approximation

$$\langle g_0(\boldsymbol{k}_F,\Omega_+ +\omega)\rangle-\langle g_0(\boldsymbol{k}_F,\Omega_+)\rangle\approx\omega d/d\Omega\langle g_0(\boldsymbol{k}_F,\Omega_+)\rangle$$

can be used.[108] For clean BCS superconductors[104] M can also be cast in the form Eq. (28) but one cannot expand the density of states around the square root singularities, which are responsible for the coherence peak in the σ_1.

The two-fluid model also breaks down when the frequency dependence of the self-energy corrections is important. There is no consistent way in which to replace $\Gamma(T)$ in Eq. (41) by some frequency averaged scattering rate. Only if ω is neglected in the denominator of Eq. (40) can we write

$$\sigma(\omega)=\frac{1}{\mu_0\lambda_p^2}\left\{\left\langle\frac{1}{2\Gamma(T,\Omega)}\right\rangle\rho_n+\frac{i}{\omega}\rho_s\right\}, \tag{45}$$

with[21]

$$\left\langle\frac{1}{\Gamma(T,\Omega)}\right\rangle=\frac{1}{\rho_n}\int_0^\infty d\Omega\frac{d}{d\Omega}\tanh\frac{\Omega}{2T}\tilde{N}(\Omega)\frac{1}{\Gamma(T,\Omega)}, \tag{46}$$

which would be less useful than Eq. (41), though.[33] A further complication is the renormalization of the London penetration depth which in strong-coupling theory is conventionally written in terms of an electron-phonon mass enhancement factor $d\tilde{\Omega}/d\Omega=1+\lambda_{\text{el-phonon}}$.[109] Hence, $\rho_n=1-\rho_s$ does not even hold for $\omega=0$. ρ_n can then only be determined from a measurement of ρ_s to within factors of 2 or 3.

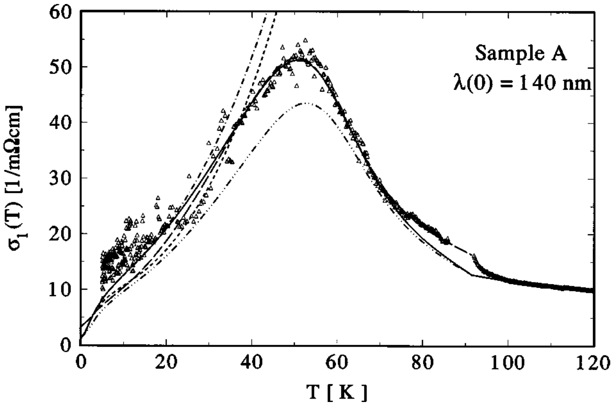

FIG. 3. Real part of the conductivity for sample A. Open triangles: experimental data, derived from the measured R_s and $\Delta\lambda$ under the assumption $\lambda(0)=140$ nm. Theoretical results based on a phenomenological inelastic-scattering rate Eq. (47),(48). Parameters are collected in Table III. Solid line: A14a; long dashed line: A14b; dot-dot-dashed line: A14c. The dot dash and short dashed lines are for $\Gamma^{\text{inel}}(T_c)=0$. The result represented by short dashes does not include the self-energy χ Eq. (24).

IV. COMPARISON BETWEEN EXPERIMENT AND THEORY

A. Phenomenological inelastic-scattering rate

Apart from the superconducting pair state, which we assume to be given by Eq. (19) unless otherwise stated, the quasiparticle-scattering rates Γ_N^{el} and Γ^{inel} are the most important material parameters determining the microwave response. As a first step we shall assume that Γ^{inel} in both the superconducting and the normal state is given by some phenomenological function of temperature, independent of frequency:

$$\Gamma^{\text{inel}}(T)=\Gamma^{\text{inel}}(T_c)f(t) \tag{47}$$

with $t=T/T_c$ the reduced temperature. Rather than trying to extract the temperature dependence of Γ^{inel} from experiment by some inversion technique,[19,26] we have varied this temperature dependence by choosing some simple functional form for $f(t)$ containing a few parameters and calculated the microwave response according to the theory outlined in the previous section. The overall size of the inelastic-scattering rate $\Gamma^{\text{inel}}(T_c)$ is determined by the conductivity at or above T_c together with the plasma wavelength λ_p Eq. (12). Based on the analysis of single-crystal data[27] we anticipate that the normal-state elastic-scattering rate Γ_N^{el} contributes only a little (less than 5%) to the total scattering above T_c, an observation made previously by Bonn *et al.*[19,26]

We begin with a discussion of the real part of the conductivity Eq. (9) which, from a theoretical point of view is the more fundamental physical quantity. In Fig. 3 we show fits of $\sigma_1(T)$ for sample A assuming $\lambda(0)=140$ nm for both the thickness correction of the experimental data and the calculation of σ_1 from Eq. (13). The elastic-scattering rate used in these calculations is $\Gamma_N^{\text{el}}=0.43$ meV corresponding to a scattering time $\tau=1.3\times 10^{-12}$ sec. Using the Fermi velocity within the $\mathrm{CuO_2}$-planes as derived from band-structure calculations,[110] $v_F\approx 2\times 10^7$ cm/sec, one obtains a mean-free path $\ell\approx 200$ nm, comparable with the penetration depth. Estimating the Fermi velocity from the slope of the upper critical field[111] reduces ℓ by almost a factor of 2. In either case, the mean-free path at $T=0$ is larger than the distance between twin boundaries which, in these well oxygenated samples, appear to be only weakly scattering. Note, that Γ_N^{el} is not the zero-temperature-scattering rate when the material becomes superconducting. This is obtained from Eq. (23) for arbitrary frequency and it can be either larger or smaller than Γ_N^{el} (cf. Fig. 14), depending on the scattering phase shift. This can also be seen from the analytic result for zero frequency Eq. (37).

Since $\lambda(0)=\lambda_p$ only holds in the clean limit,[102] one has to readjust λ_p every time Γ_N^{el} or δ_N are changed in order to obtain theoretical curves consistent with a particular choice of $\lambda(0)$. Having thus fixed λ_p one could, in principle, determine $\Gamma^{\mathrm{inel}}(T_c)$ from $\sigma_1(T_c)$ according to Eq. (39). Unfortunately, an accurate value for $\sigma_1(T_c)$ cannot be extracted from our measurements, as will be discussed below. One reasonable method for determining $\Gamma^{\mathrm{inel}}(T_c)$ would be to fit as much of the data taken in the TE_{013} mode as possible. This would yield $\Gamma^{\mathrm{inel}}(T_c)=8.6$ meV (Fig. 3, long dashed line). On the other hand, from around 100 K to the maximum temperature of 145 K at which data were taken, $\sigma_1(T)$ is compatible with choosing $f(t)=t$ in Eq. (47). An explanation for this temperature dependence can be found in terms of the spin fluctuation exchange between quasiparticles in some tight binding band,[42] a simplified description of which is provided by the NFL model[60] (see previous section). This approach gives in the present case $\Gamma^{\mathrm{inel}}(T_c)=10.95$ meV rather than 8.6 meV (Fig. 3, solid line).

Since for a d-wave superconductor $\Gamma^{\mathrm{inel}}(T)$ must drop rapidly below T_c in order to account for a peak in σ_1, the small elastic-scattering rate has a significant influence up to temperatures around 75 K. On the other hand, the effect of Γ^{inel} becomes negligible only when $T \leqslant 25$ K so that over most of the temperature range both types of scattering play an important role. This is demonstrated in Fig. 3 by the dot-dashed curve, which results when the inelastic scattering used to calculate the full curve is set equal to zero. When, furthermore, the self-energy χ Eq. (24) is omitted from the calculation of σ_1, the short dashed curve is obtained. Agreement between theory and experiment can be restored simply by reducing Γ_N^{el} to 0.32 meV without changing $\Gamma^{\mathrm{inel}}(T)$ significantly.[112] It thus seems that the omission of χ only leads to an error in the some of the fit parameters, which would not be very relevant. The effect of χ on σ_1 is, however, strongly frequency dependent and we shall return to a discussion of this point below (see Fig. 10). The dot-dot-dashed line in Fig. 3 shows the effect of a change in $\lambda(0)$ on the calculated conductivity. It will be discussed in connection with Fig. 6.

The two fits to the experimental data shown in Fig. 3 differ not only in the choice of $\Gamma^{\mathrm{inel}}(T_c)$ but also in the choice of scattering phase shift. Note, that the sizable conductivity observed at around 4 K can be explained without invoking extrinsic effects if the scattering phase shift is suitably chosen. To further elucidate the importance of the phase shift δ_N we compare in Fig. 4(a) the low-temperature behavior of $\sigma_1(T)$ calculated for various values of δ_N with the experimental results. Other parameters are the same as those for the solid curve in Fig. 3. Keeping $\lambda_p=134.6$ nm fixed while δ_N is varied causes $\lambda(0)$ to increase from 136.0 to 144.2 nm. Readjusting parameters such that $\lambda(0)$ is kept constant has a visible but very small effect on the curves shown in Fig. 4(a).

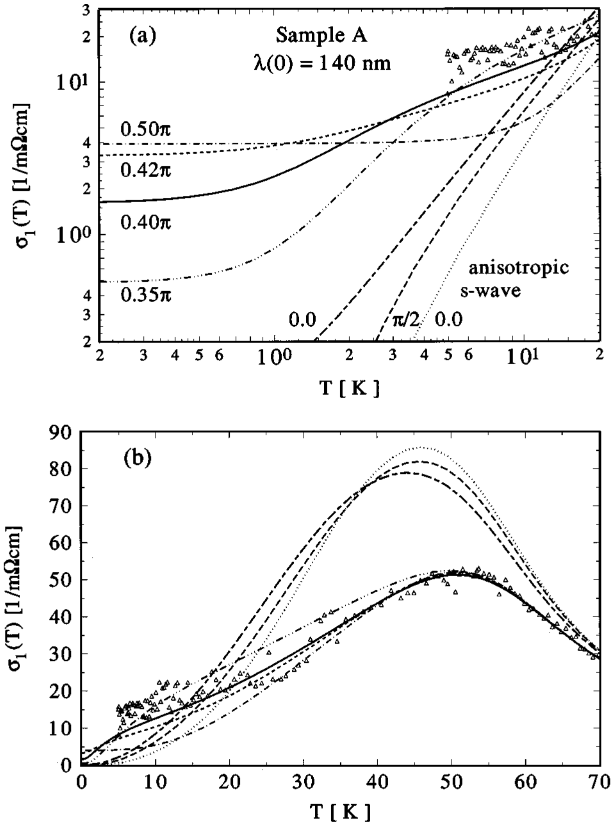

FIG. 4. Effect of the scattering phase shift on the temperature dependence of the real part of the conductivity at very low temperatures [panel (a)] and over a broad temperature range [panel (b)]. Also included are results for the anisotropic s-wave state $\Delta_0(T)|\cos 2\varphi|$ Eq. (20a). Except for the variable phase shift the parameter set A14a has been used in all calculations.

Clearly, the zero-temperature conductivity is by no means universal[103,21,98] because, as discussed in the previous section, the frequency used in the experiment is small compared to the zero-temperature-scattering rate only for $\delta_N \approx 0.5\pi$. It is only the unitarity limit $\sigma_1(T=0,\delta_N=0.5\pi) = 3.89[\mathrm{m}\Omega\ \mathrm{cm}]^{-1}$ in Fig. 4 which agrees very closely with Eq. (34). For fixed frequency and given phase shift the deviation from this universal conductivity decreases with increasing Γ_N^{el}.[112] It is due to the small values of Γ_N^{el}, comparable with the microwave frequency, that small changes in δ_N have sizable effects on $\sigma_1(T=0)$.[112] The monotonic decrease of $\sigma_1(T=0)$ with decreasing phase shift has been reported earlier by some of the present authors.[36] As in previous experiments[19,27,26] the ''universal'' conductivity Eq. (34) is too small to be compatible with the data taken at the lowest temperatures. However, away from the unitarity limit, $\sigma_1(T,\delta_N)$ acquires a strong temperature dependence so that it can exceed $\sigma_1(T=0,\delta_N=0.5\pi)$ at temperatures as low as 4 K in close agreement with the data. If this interpretation is correct, $\sigma_1(T)$ and $R_s(T)$ would have to decrease by at least an order of magnitude between 0.4 and 4 K.

In Fig. 4(b) we show the same theoretical results as in

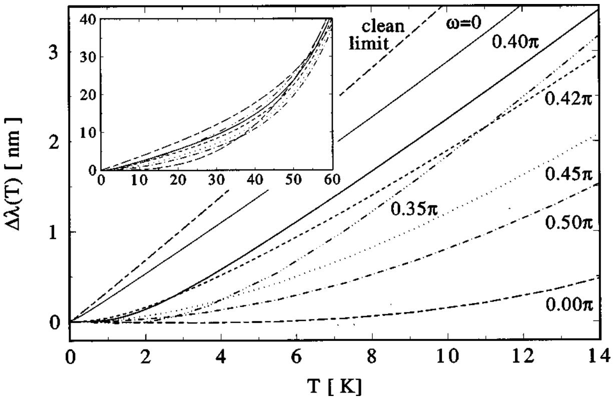

FIG. 5. Effect of the scattering phase shift on the temperature dependence of the penetration depth at 87 GHz. Except for the variable phase shift the same parameter set A14a as in the previous figure has been used in all calculations. Also shown is the clean limit zero-frequency result (alt. dashed line). The only difference between the two solid curves is the frequency ($\omega=0$ for the thin solid line).

Fig. 4(a) but for a wider temperature range using a linear scale. Note that in both limiting cases $\delta_N=0$ and $\delta_N=\pi/2$ the conductivity seems to vary quadratically with temperature at low temperatures, contrary to experimental observation. In Fig. 4 results for the anisotropic s-wave state Eq. (20a) are included. Within the present weak-coupling treatment of the inelastic scattering, σ_1 for this particular s-wave state would coincide with the d-wave results for $\Gamma_N^{\mathrm{el}}=0$. For $\Gamma_N^{\mathrm{el}}=0.43$ meV and δ_N arbitrary, the s-wave results are still close to the weak-scattering limit of the d-wave model as discussed above Eq. (28). This variation of σ_1 with Γ_N^{el} and δ_N for the two states is related to the difference in the changes to the density of states (DOS) at low energies induced by scattering.[50–52] The remarkable conclusion to be drawn from Fig. 4 is that assuming the s-wave state Eq. (20a) one cannot fit the low-temperature data for any scattering phase shift even though Γ_N^{el} is so small that its effect on the DOS is almost invisible and certainly not observable using tunneling, angle-resolved photoemission spectroscopy (ARPES), or specific-heat measurements.

The scattering phase shift δ_N also has quite a dramatic effect on the temperature dependence of $\Delta\lambda(T)$ as shown in Fig. 5. As in Fig. 4 the normal-state parameters including λ_p are the same for all the curves shown. Again, it is only at rather high temperatures $T\approx 80$ K that elastic scattering becomes negligible and the six curves shown for $f=87$ GHz and $\Gamma_N^{\mathrm{el}}=0.43$ meV coalesce into one. As a kind of reference point we included in Fig. 5 the change in penetration depth at zero frequency in the clean limit, given at low temperatures by Eqs. (43) and (44). In this case, the slope of $\Delta\lambda(T)$ is given by $\ln 2\lambda_p/\Delta_0(0)$. In the temperature regime shown, finite frequencies[21,33] and mean-free path effects reduce $\Delta\lambda$ to below this limiting curve. Note, that the dependence of $\Delta\lambda(T)$ on δ_N is far from monotonic. This nonmonotonic behavior is a consequence of the finite experimental frequency used in the calculations. For the range of elastic-scattering rates considered here, $\Delta\lambda(T,\omega=0)$ is nearly independent of Γ_N^{el} in the weak-scattering limit $\delta_N=0$, because the relevant average scattering rate (see Figs. 15 and 18) is less than (π times) the experimental frequency and we have reached the relaxation regime.[107] In the unitarity limit $\delta_N=0.5\pi$ it is very different from the clean limit zero-frequency curve shown but it does not vary appreciably with frequency. Introducing comparatively weak-scattering $\delta_N=0.4\pi$ at $\omega=0$ changes the limiting curve to the thin solid line. Including a finite frequency no greater than the relevant scattering rate again causes only small changes to $\Delta\lambda(T)$. This is why for $\delta_N\approx 0.4\pi$ we find a nearly linear temperature dependence except at very low temperatures. With no experimental data available at those low temperatures, with $\Delta_0(0)$ as fit parameter, and bearing in mind the uncertainty in $\lambda(0)$, this temperature dependence can hardly be distinguished from the zero-frequency clean limit result.

A frequency dependence of $\Delta\lambda(T)$ has been observed by Dähne *et al.*[33] and by Vaulchier *et al.*[35] Part of the frequency dependence is simply due to the fact that $\lambda(T_c)\propto 1/\sqrt{\omega}$. The temperature variation measured by Dähne *et al.* at 300 GHz seems to be negligible below 50 K, which the authors interpret as an indication for the relaxation regime [see discussion below Eq. (44)]. In contrast, the temperature dependence observed by Vaulchier *et al.* at frequencies varying from 120 to 510 GHz is linear up to 40 K with a slope that is similar to that of the $\delta_N=0.4\pi$ curve shown in Fig. 5. It has been suggested by Bonn and Hardy[23] that the different observations could be attributed to a difference in the elastic-scattering rates. To account for the linear temperature dependence in the presence of substantial elastic scattering one would again have to invoke finite-scattering phase shifts. For a discussion of the variability with sample quality see Ref. 112 and below.

Since precision measurements of $\Delta\lambda(T,\omega=0)$ appear to be possible,[113] there is hope that this d-wave model can be further tested by measuring the curvature of $\Delta\lambda(T,\omega=0)$ always to be expected at very low temperatures. Experimental data obtained with this method for $YBa_2Cu_3O_{7-\delta}$ (7 K $\leqslant T\leqslant$58 K) and $La_{1.85}Sr_{0.15}CuO_{4-\delta}$ (4.2 K$\leqslant T\leqslant$16.5 K) can be explained satisfactorily within this model with parameters consistent with those used in the present paper.[114,115] The results obtained for $\Delta\lambda(T)$ using the anisotropic s-wave state Eq. (20a) are again very close to the weak-scattering result of the d-wave model.

Just below T_c, $\sigma_1(T)$ (Fig. 3) shows positive curvature rather than the large discontinuous change in slope and negative curvature characteristic of the coherence peak.[116] This feature can only be reproduced by the present model if $f(t)$ displays a more or less pronounced S shape. A simple function that can be used to model such behavior is

$$f(t;a,b_1,b_2)=at^3+(1-a)e^{b_1(t-1)[1+b_2(t-1)^2]}. \tag{48a}$$

A temperature dependence $\exp(b_1t)$ has been extracted by Bonn *et al.* from their experimental data using a two-fluid model.[19] This kind of T dependence might seem somewhat unusual, but it is very similar to a perhaps more familiar functional form

$$f(t;a,b_1',b_2')=at^3+(1-a)e^{b_1'(1-1/t^{b_2'})} \tag{48b}$$

except at very low temperatures, where the form of $f(t)$ is irrelevant because Γ_N^{el} dominates. A t^3 term has been included in view of Eq. (32). This term becomes comparable with the exponential contribution to $f(t)$ at around the temperature at which the peak occurs. Its size is, therefore, important in determining the peak height and the peak position. In order for the T dependence below the peak to be unaffected by different choices of $\Gamma^{\mathrm{inel}}(T_c)$, this cubic term has to remain unchanged, i.e., $\Gamma^{\mathrm{inel}}(T_c)a=\mathrm{const}$. The values of a used in Fig. 3 have been chosen in accord with this condition. The expression Eq. (48b) has the advantage of vanishing exponentially at $T=0$ rather than showing a linear approach to a finite value which, for small enough b_2, might dominate the T^3 behavior.

Obtaining a good fit to the conductivity cannot be hailed as a great success of this theory considering that we had not just a few parameters but a function $\Gamma^{\mathrm{inel}}(T)$ at our disposal to optimize the fit. Except for conclusions drawn from the quality of the fit at very low temperatures, where $\Gamma^{\mathrm{inel}}(T)$ does not contribute, it is this function itself that provides some interesting insight into the properties of high-temperature superconductors. We shall return to this point in the next subsection. However, according to Eq. (10) the experimentally determined σ_1 depends strongly on the plasma wavelength λ_p Eq. (12), or the London penetration depth $\lambda(0)$ resulting from it, and we need to examine how $\Gamma^{\mathrm{inel}}(T)$ as well as the other parameters determined from the fit are affected by the choice of λ_p. FIR reflectivity measurements on untwinned crystals give $\lambda(0)\approx 140$ nm for the average penetration depth and $\lambda(0)\approx 160$ nm for the direction not involving the CuO chains.[31] μSR experiments on single crystals yield an average $\lambda(0)$ in the range 145 to 150 nm,[30] while transmission experiments on thin films at a number of microwave frequencies give a minimum $\lambda(0)\approx 175$ nm for films of the highest quality. In order to assess the effect a change in $\lambda(0)$ has on $\Gamma^{\mathrm{inel}}(T)$ and on the other parameters required to fit $\sigma_1(T)$, we also chose the value $\lambda(0)=160$ nm to correct the experimental data for the finite film thickness. This does not affect the value of the normal-state conductivity Eq. (39) derived from the measured surface resistance using the assumption $R_s=X_s$ (see Sec. II). Increasing $\lambda(0)$ thus means that a lower normal-state scattering rate has to be assumed.

The dot-dot-dashed curve in Fig. 3 shows the effect of increasing $\lambda(0)$ to ≈ 160 nm. To keep $\sigma_1(T_c)$ unchanged we had to take $\Gamma^{\mathrm{inel}}(T_c)=8.3$ meV. All other parameters are the same as for the solid curve. With the change in λ_p compensated above T_c by a different choice of $\Gamma^{\mathrm{inel}}(T_c)$, there is very little change in the temperature regime where inelastic scattering dominates. Starting at T_c with a lower value of the inelastic-scattering rate, effects resulting from the reduction of Γ^{inel} due to the onset of superconductivity must become less pronounced and thus a reduction of the peak height of σ_1 follows naturally. At low temperatures, where Γ^{inel} does not contribute significantly, the theoretical result for σ_1 is according to Eqs. (13) and (34) proportional to λ_p^{-2}, when all other parameters are held fixed. The experimental results for R_s are affected by the choice of λ_p only through the corrections required to account for the finite film thickness. At low temperatures these corrections are very small and at elevated temperatures at which $\lambda(T)$ is large, a change in $\lambda(0)$ only leads to small modifications of these corrections. In view of Eq. (10) we, therefore, expect that σ_1 as derived from the measured R_s will decrease as λ_p^{-3} and thus will turn out to be smaller than can be accounted for by a corresponding increase of λ_p in the calculations. This is clearly visible in Fig. 6 where the data points fall well below the dot-dot-dashed curve from Fig. 3. Obviously, the whole set of parameters used in Fig. 3 needs to be readjusted to obtain a good fit. The reduction in peak height relative to the dot-dot-dashed curve could be modeled by an increase in both Γ_N^{el} and $\Gamma^{\mathrm{inel}}(T<T_c)$ (parameter set A16a, Table III) or by an increase of the order-parameter amplitude, which would cause the number of occupied quasiparticle states to decrease more rapidly with decreasing temperature. The curve corresponding to the parameter set A16a is not shown in Fig. 6. It is practically identical with the solid curve except below ≈ 25 K where it deviates to slightly higher values of σ_1. The order-parameter amplitude cannot be increased arbitrarily. According to Eq. (34) we expect $R_s(T=0)\propto\lambda_p/\Delta_0(0)$. Hence, to retain the agreement with the experimentally determined R_s resulting from the choice of parameters used in Fig. 3, we have to keep this ratio approximately constant. This brings $2\Delta_0(0)/kT_c$ into the vicinity of 6.8 rather than 6.0.

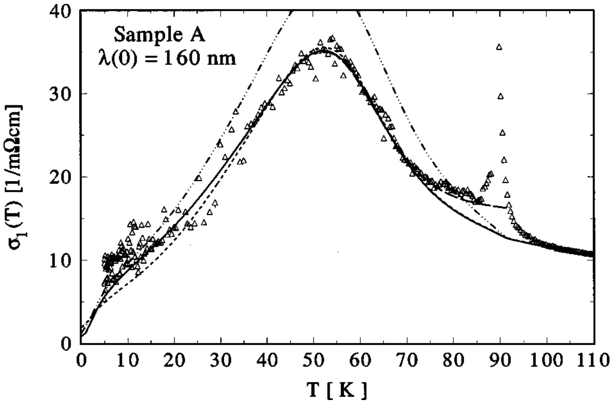

FIG. 6. Real part of the conductivity for sample A. Open triangles: experimental data, derived from the measured R_s and $\Delta\lambda$ under the assumption $\lambda(0)=160$ nm. Theoretical results based on a phenomenological inelastic-scattering rate Eq. (47),(48). Parameters are collected in Table III. Solid line: A16b; short dashed line: A16c; long dashed line: A16d. The dot-dot-dashed line is identical to the one shown in Fig. 3.

The real part of the microwave conductivity discussed so far is not measured directly but has to be extracted from the measured surface impedance according to Eq. (9) and errors in the surface resistance and penetration depth data appear greatly enhanced in $\sigma_1(T)$. Furthermore, rather different parameter sets will produce the same $\sigma_1(T)$ curves. The true quality of the fits can, therefore, only be assessed when the experimental results for both R_s and $\Delta\lambda$ are compared with the theory. It can be hoped that at the same time the range of parameters compatible with $\sigma_1(T)$ is greatly reduced. Figure 7 shows the temperature dependence of the penetration depth $\lambda(T)$ for the two choices of $\lambda(0)$. Since the increase in $\lambda(T)$ between $T=0$ and the lowest temperatures $T_{\mathrm{min}}\approx 4$ K at which data have been taken is not negligible according to

TABLE III. Parameter sets used to generate theoretical fits assuming a phenomenological inelastic-scattering rate.

Parameter set	Γ_N^{el} [meV]	δ_N	$\Gamma^{\mathrm{inel}}(T_c)$ [meV]	a	b_1	b_2	$\frac{2\Delta_0(0)}{kT_c}$	λ_p[nm]	$\lambda(0)$ [nm]
A14a	0.43	0.40π	10.95	0.14	6.3	4.0	6.0	134.6	140.00
A14b	0.43	0.42π	8.6	0.18	5.0	5.5	6.0	133.4	139.99
A14c	0.43	0.40π	8.3	0.14	6.3	4.0	6.0	154.0	160.18
A16a	0.57	0.39π	8.4	0.18	5.0	6.2	6.0	152.5	159.97
A16b	0.43	0.40π	8.25	0.15	5.5	5.0	6.8	154.7	160.16
A16c	0.43	0.42π	8.38	0.15	5.5	5.0	6.8	153.3	160.01
A16d	0.43	0.40π	6.3	0.20	4.0	8.0	6.8	154.7	160.25
B14a	0.20	0.40π	9.30	0.00	7.4	1.2	5.6	137.3	140.02
B14b	0.10	0.42π	9.0	0.00	8.5	0.8	6.8	138.6	139.97
B16a	0.11	0.44π	6.9	0.00	7.4	1.2	7.4	158.0	160.10
B16b	0.11	0.43π	6.9	0.12	7.9	2.7	7.4	158.2	160.01

our calculations, we have attributed a finite value to $\Delta\lambda(T_{\min})$ so as to optimize the fit. For both choices of $\lambda(0)$ excellent fits can be obtained for temperatures up to around 70 K, but only if different values of $\Delta_0(0)$ are used.

Between 10 and 45 K the data seem to vary more linearly with temperature than predicted by our theory. The rather distinct change in the slope of $\lambda(T)$ at $T\approx 50$ K is also not quite accurately reproduced by the present theory. Since around 50 K is the temperature regime with the largest relative error one cannot conclude that this disagreement is significant. However, such a kink in $\lambda(T)$ appears to be regularly observed in this kind of experiment. It has been attributed to a second superconducting gap opening up at this temperature.[14]

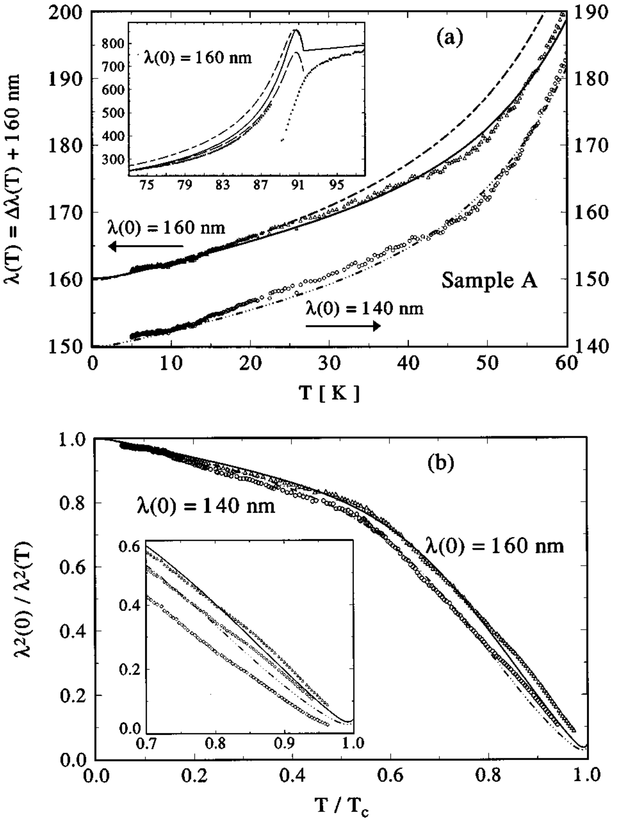

FIG. 7. Temperature dependence of the penetration depth $\lambda(T)$ for the two choices of $\lambda(0)$. To obtain the solid and the dot-dot-dashed curves, the same parameter sets that gave good fits to σ_1 in Figs. 3 and 6 have been used (A16b and A14a, respectively). Alternate dashed line: A16a; long dashed line in the inset: A16d. In panel (b) these results are replotted in the form of a superfluid density. The inset shows the temperature regime near T_c to facilitate the discussion of fluctuation effects.

Below T_c the experimental data taken with the TE_{013} mode fall well below the calculated curves [Fig. 7(a), inset]. As the comparison between the curves for $2\Delta(0)/kT_c = 6.0$ (alt. dashed) and $2\Delta(0)/kT_c = 6.8$ (solid) shows, agreement could be improved by substantially increasing the order-parameter amplitude, but this would not allow us to interpret the data below 70 K in terms of the present theory. Alternatively, good agreement could be achieved at all temperatures if T_c would be increased by 0.9 K. This, however, is not compatible with the T_c determined independently (see Sec. II A) which also gives a good fit to the surface resistance.

Well above T_c it is safe to assume that σ is real, the imaginary part arising from the finite frequency being negligible. In this normal skin effect regime both λ and R_s can be determined from a measurement of the quality factor by imposing a condition of self-consistency when correcting for finite film thicknesses. The penetration depth obtained in this way from measurements with the TE_{021} mode does not involve estimates of $\lambda(0)$. These data points clearly do not match the penetration depth obtained with the TE_{013} mode [Fig. 7(a), inset]. It is highly unlikely that the drop in $\lambda(T) = R_s/\omega\mu_0$ can be attributed solely to a deviation of the scattering rate from its T-linear behavior. An increase in σ_1 in this temperature regime is more likely attributable to fluctuations[117–119] or inhomogeneities,[120,121] but both these mechanisms for increasing σ_1 necessarily render σ complex. When σ acquires an imaginary part, R_s drops but $\lambda(T,\omega)$ can develop a peak, as was predicted some time ago.[122] As long as the local limit can be used in the calculation of the surface impedance we have from Eq. (8)

$$\sqrt{2\omega\mu_0}\lambda = \frac{1}{\sqrt{\sigma_1^2+\sigma_2^2}}\sqrt{\sqrt{\sigma_1^2+\sigma_2^2}+\sigma_2}, \tag{49}$$

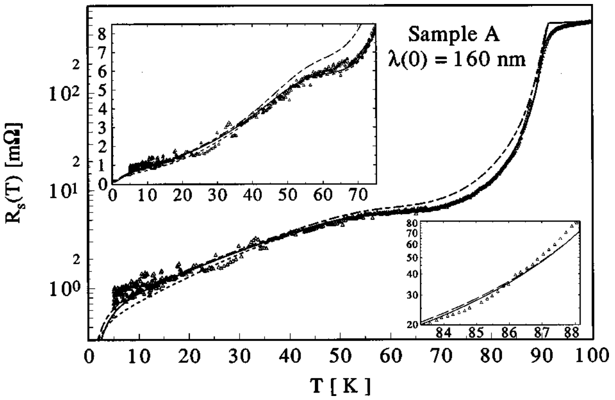

FIG. 8. Surface resistance of sample A obtained from the measured effective surface resistance under the assumption $\lambda(0)=160$ nm. Main frame: semilogarithmic plot; upper left inset: linear plot of R_s at low temperatures; lower right inset: blowup of $R_s(T)$ at the highest temperatures at which data are taken in the TE_{013} mode, showing some evidence for fluctuation effects. The coordination between symbols and parameter sets is the same as in Figs. 6 and 7. Solid line: A16b; short dashed line: A16c; alt. dashed line: A16a; long dashed line: A16d.

independent of any particular theory of the superconducting state. Expanding this expression close to T_c around the normal-state conductivity $\sigma_N(\omega=0)$ assuming $\sigma_2 \ll \sigma_N$ and $\delta\sigma_1=\sigma_1-\sigma_N \ll \sigma_N$ we find

$$\sqrt{2\omega\mu_0}\lambda=\frac{1}{\sqrt{\sigma_N}}\left(1+\frac{\sigma_2}{2\sigma_N}-\frac{\delta\sigma_1}{2\sigma_N}\right) \tag{50}$$

so that the penetration depth increases below T_c provided σ_2 increases faster than σ_1. Such a peak has been observed in strong-coupling conventional superconductors tantalum and niobium[122,123] and in the unconventional superconductor UPt$_3$.[124] In more recent work on UPt$_3$ this peak was found to be sample dependent.[125] For unconventional superconductors the purity dependence of the peak has been discussed by Hirschfeld *et al.*[126] For a d-wave superconductor σ_1 does not change very much near T_c so that a sizable peak in $\lambda(T)$ results as shown in the inset of Fig. 7(a). When the increase in σ_1 due to fluctuations[117–119] or inhomogeneities[120,121] is taken into account, the peak should be reduced. If, furthermore, a finite value of σ_2 above T_c were included in the theory, the peak would shift to higher temperatures. This would lead to an improved agreement between theory and experiment in the temperature range 70 K$\leq T \leq$88 K.

Above 88 K $\lambda(T)$ is not measured, but we need an estimate of this quantity to correct R_s for finite film thicknesses. When $\lambda(T)=R_s/\omega\mu_0$ is used, the sets of R_s data obtained using the two modes cannot be smoothly joined after they have been corrected. We incorporated an imaginary contribution to σ by simply extrapolating $\lambda(T)$ derived at $T\geq 110$ K linearly to lower temperatures. This crude guess yields much better agreement between the two data sets, permitting a determination of T_c from the microwave surface resistance (Fig. 8). The result is in good agreement with the value measured inductively (see Sec. II A).

Knowledge of $\lambda(T)$ is also required in order to obtain $\sigma_1(T)$. The sharp rise in σ_1 (Fig. 6) as the cavity mode switch point is approached from above simply reflects the very low $\lambda(T)$ values shown in the inset of Fig. 7(a). With the above modification of $\lambda(T)$ a very different $\sigma_1(T)$ results. It is, therefore, not possible to learn anything about fluctuations from the present experiments, except where the data have been taken with the TE_{013} mode. On the contrary, we would require a thorough understanding of fluctuation in d-wave superconductors to complement our experimental data in the vicinity of T_c.

A difference in the choice of $\lambda(0)$ becomes most apparent, when the superfluid density $\lambda^2(0)/\lambda^2(T)$ is plotted [Fig. 7(b)]. This type of plot is also useful to elucidate the temperature dependence of the penetration depth near T_c. For $T\geq 0.8T_c$ the superfluid density seems to deviate from the mean-field result in much the same way as has recently been reported by Anlage *et al.*[119] However, above $0.88T_c$ our data extrapolate linearly to zero, rather than bending downwards to the finite value expected at this frequency [Fig. 7(b), inset]. Consequently, when the data for $\lambda(0)=160$ nm are replotted as $\lambda^3(0)/\lambda^3(T)$ (open diamonds), the resulting curve shows positive curvature. This behavior is influenced by the choice of the mean field T_c as discussed below.

In Fig. 8 we compare the measured surface resistance with theory using a logarithmic scale, while in the upper left inset the same comparison is presented for $T\leq 75$ K using a linear scale. The figure demonstrates that an excellent fit for R_s can be obtained over the whole temperature range and covering three decades with the parameters set A16b in Table III (solid curve). As with the penetration depth, choosing $\lambda(0)=140$ nm does not affect the quality of the fit when the remaining parameters are suitably adjusted. We, therefore, only show results for $\lambda(0)=160$ nm. $\Gamma^{\mathrm{inel}}(T_c)$ has been chosen such that the normal-state data are reproduced.

The parameter set A16a (alt. dashed curve) with its small order-parameter amplitude does not give a satisfactory fit for $T\geq 40$ K. This shows that parameters can be found which fit one quantity, in this case σ_1, very well but fail dismally when used to evaluate other, related quantities. The sharp drop in R_s below T_c does not depend sensitively on the pair state. Even an isotropic s-wave state would give a very similar result. The most important parameter here is the order-parameter amplitude $\Delta_0(T)$ whose temperature dependence in weak coupling is very nearly the same for a large range of unconventional and conventional pair states when normalized to $\Delta_0(0)$. A smaller value of $\Delta_0(0)$ could fit the data provided $\Delta_0(T)$ increases more rapidly below T_c than predicted by weak-coupling theory. Modeling such ''strong-coupling'' behavior introduces additional parameters, so we decided not to pursue this idea here.[61]

As with $\sigma_1(T)$, theory predicts a further substantial decrease of R_s at temperatures below those reached in the experiment. An increase in the scattering phase shift (A16c, short dashed curve), which would be consistent with the observed $\lambda(T)$, leads to too small values of R_s at low temperatures (cf. Fig. 8).

For T_c we have used the value 91.6 K determined independently (see Sec. II A). The rounding of R_s near T_c is, of course, not reproduced by the present theory. In order to correlate the unexplained features in σ_1 (Fig. 6) with the actual experimental results, we show in the lower right inset of Fig. 8 a blowup of the last data points obtained with the

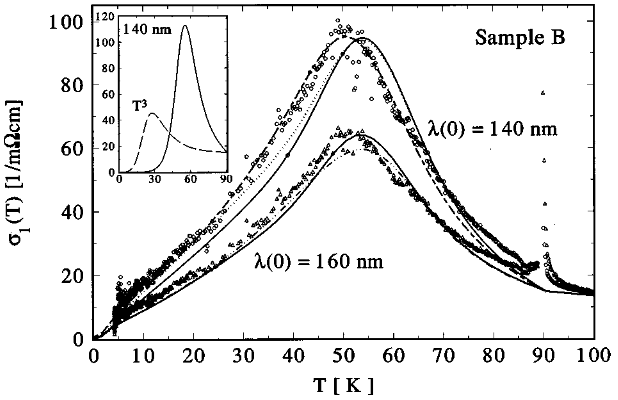

FIG. 9. Real part of the conductivity for sample B for two choices of $\lambda(0)$. Parameter sets are given in Table III. $\lambda(0)=140$ nm. Alt. dashed line: B14a; solid line: B14b. The dotted line is obtained when the self-energy χ Eq. (24) is neglected. $\lambda(0)=160$ nm. Solid line: B16a; dot-dot-dashed line: B16b. The inset shows the conductivity in the absence of elastic scattering. The solid curve is based on the same temperature-dependent inelastic-scattering rate as the corresponding solid curve in the main frame of the figure. To obtain the long dashed curve we assumed the inelastic-scattering rate to vary $\propto T^3$.

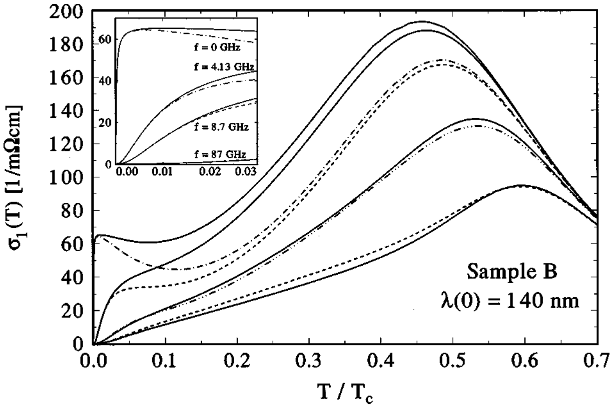

FIG. 10. Effect of the self-energy χ Eq. (24) on the real part of the conductivity for different frequencies. Other parameters are as defined in the set B14b (Table III). The frequencies in the main frame are 0 GHz, 8.7 GHz, 43.5 GHz, and 87 GHz (from top to bottom). The inset shows the variation of $\sigma_1(T)$ at very low reduced temperatures.

TE_{013} mode. There is a distinct change in slope at 85 K which is responsible for the sharp upturn in σ_1 below the cavity mode switching point. Otherwise, theoretical results are well within the error margins of the experiment. $\lambda(T)$ [Fig. 7(a), inset] shows no significant change at 85 K. The discrepancy between theory and experiment narrows very gradually over a much wider temperature range. This raises the question of whether two different physical effects come into play here. In view of the small transition width $\Delta T_c=1.6$ K observed in the inductive measurement of T_c it seems unlikely that inhomogeneities[120,121] can explain a conductivity peak extending down to 85 K so that one would look for fluctuations[117–119] as a possible explanation. With our choice of T_c the discrepancy between the values of σ_1, as derived from $\Delta\lambda(T)$ and $R_s(T)$, and theory for temperatures 72 K$\leqslant T \leqslant$85 K has to be attributed to our failure to produce accurate fits to $\lambda(T)$ in this temperature range. If we were to adopt a slightly higher transition temperature, the discrepancy between theory and experiment could be distributed evenly between $\lambda(T)$ and $R_s(T)$.

Choosing parameter set A16d (long dashed curves), which fits σ_1 for all $T \leqslant 85$ K (Fig. 6), gives much improved agreement for $\lambda(T)$ [Fig. 7(a), inset] without significantly altering the fit to $R_s(T)$ (Fig. 8, lower right inset). This shows that with $\Gamma^{\mathrm{inel}}(T_c)$ as an additional adjustable parameter we can fit all the data below 88 K very well indeed. The fact that in the transition region this simple theory meets with some difficulty would have escaped our notice had we not tried to incorporate the normal state.

We now turn to sample B, which has a smaller resistance at T_c corresponding to $\Gamma^{\mathrm{inel}}(T_c)=9.3$ meV rather than $\Gamma^{\mathrm{inel}}(T_c)=10.95$ meV. The real part of the conductivity is shown for two choices of $\lambda(0)$ in Fig. 9. The conductivity peaks are at the same position as those obtained for sample A but they are much higher. The high peak resulting from $\lambda(0)=140$ nm can be reproduced theoretically by using a rather small order-parameter amplitude $2\Delta_0(0)/kT_c=5.6$, even smaller than the one used in Fig. 3, and an elastic scattering rate reduced by about a factor of 2 (parameter set B14a, Table III, alt. dash curve). It turns out, though, that these parameters fit neither $R_s(T)$ nor $\lambda(T)$. The fits for these quantities can only be improved by increasing $\Delta_0(0)$. It might seem possible that the resulting loss in quasiparticle number can always be compensated by further reducing the scattering rates. If the relevant scattering rate drops below the external frequency, though, σ_1 *decreases* with decreasing Γ because the quasiparticles still present form a more ideally conducting system.[107] So, for fixed frequency and a more and more rapidly decreasing scattering rate the peak height increases but at the same time shifts to higher temperatures. The inset of Fig. 9 shows σ_1 when only the temperature-dependent scattering rate Eq. (47) is included. The solid curve is obtained with the exponentially decreasing function $\Gamma^{\mathrm{inel}}(T)$ that was used to calculate the corresponding curve in the main part of the figure. The long dashed curve results if we only keep the cubic term in Eq. (48). We see that peak height and peak position of σ_1 cannot be reproduced simultaneously with great accuracy by simply manipulating $\Gamma^{\mathrm{inel}}(T)$.

At the small elastic-scattering rate required for this fit, taking the self-energy part χ Eq. (24) into account actually diminishes the agreement between theory and experiment. The dotted curve is calculated without χ. To study the effect of χ in more detail we calculated σ_1 for various frequencies using the parameter set B14b that gives the solid curve in Fig. 9. Figure 10 demonstrates that χ becomes very important at this low value of $\Gamma_N^{\mathrm{el}}=0.10$ meV for frequencies less than 10 GHz. The inset shows that χ has no effect on σ_1 at very low temperatures. The intrinsic temperature dependence of $\chi(T,\Omega)$ is negligible at least up to $T\approx 0.7T_c$ but the range of frequencies contributing to the integral Eq. (13) increases with temperature. Even though $\mathrm{Im}\chi(T,\Omega=0)$ vanishes, we obtain a large contribution from $\mathrm{Im}\chi$ in the last term of Eq. (13). $\mathrm{Re}[\chi(\Omega)-\chi(\Omega+\omega)]$ drops out of Eq. (16) at any temperature for small external frequency but can become comparable to the contribution from $\mathrm{Im}\chi$ at the frequency used in our experiment. The low frequency results without

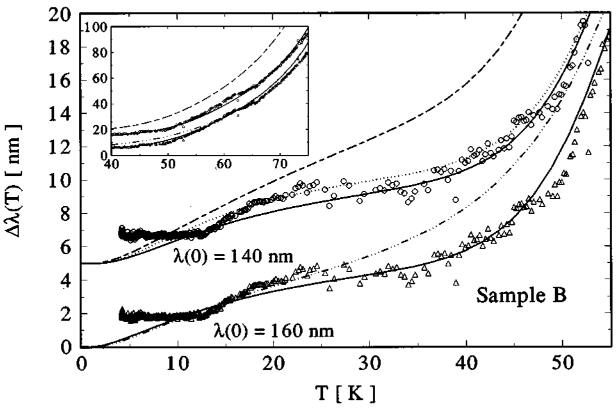

FIG. 11. Temperature dependence of the penetration depth $\lambda(T)$ for the two choices of $\lambda(0)$. For clarity, results for $\lambda(0)=140$ nm have been shifted upwards by 5 nm (10 nm in the inset). Parameters for the theoretical curves are the same as those in Fig. 9.

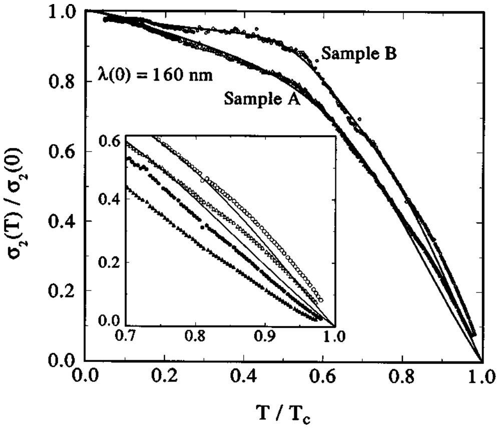

FIG. 12. Comparison of the imaginary parts of the conductivities for the two samples. Solid lines: parameter sets A16b and B16a, respectively. Dot-dot-dashed line: B16b. The inset shows the temperature regime near T_c. As compared to Fig. 7, T_c for sample A has been reduced to 90.5 K. Full symbols in the inset are data points replotted as $\lambda^3(0)/\lambda^3(T)$.

χ taken into account agree with a curve published by Borkowski *et al.*[89] in their Fig. 5. Such a plateau or minimum in $\sigma_1(T)$ is incompatible with the low-frequency measurements of Bonn *et al.*[19,26] and Jacobs *et al.*[27]

Note that the conclusion $R_s \propto \omega^2$ derived from Eq. (10) requires σ_1 to be frequency independent. According to the present theory this conclusion is expected to break down in the GHz regime at sufficiently low temperatures. This breakdown is again related to the relevant scattering rate becoming comparable to the external frequency. A better fit to $\sigma_1(T)$ as well as $R_s(T)$ and $\Delta\lambda(T)$ can be obtained if we choose $\lambda(0)=160$ nm and increase the order-parameter amplitude. Including a cubic term in $\Gamma^{\text{inel}}(T)$ improves agreement around 35 K but fails to give the correct peak height (cf. Fig. 9).

The penetration depth (Fig. 11) can be reproduced very well if the T^3 contribution to $\Gamma^{\text{inel}}(T)$ is negligible (solid curves). The effect of χ on $\Delta\lambda(T)$ (dotted curve) is within experimental error. Including a T^3 contribution (dot-dot-dashed curve) does not allow us to reproduce the rather sharp kink in $\Delta\lambda(T)$ at around 45 K which is much more pronounced in sample B and which is responsible for the large conductivity peak. The inset shows that the discrepancy between this curve and the data only extends over a limited temperature regime. Assuming a smaller order-parameter amplitude that perfectly fits σ_1 results in the alt. dashed curve which, even allowing for rather wide error margins, disagrees with the data for all temperatures above 20 K. For temperatures above 75 K the calculated curves give $\Delta\lambda(T)$ larger than has been observed for reasons already discussed in connection with sample A.

In Fig. 12 we compare the imaginary parts of the conductivities of the two samples. This quantity is more closely related to the superfluid density than $\lambda^2(0)/\lambda^2(T)$ as obtained from Eq. (8). Due to the finite frequency, even σ_2 does not vanish in the normal state, but it is more than an order of magnitude smaller than the inverse square of the normal-state penetration depth (skin depth) and thus appears to vanish at T_c. The finite value followed by a dip shown in Fig. 7(b) is, therefore, absent when the results are plotted in this form. The difference between those two ways of plotting the data, both experimental and theoretical, becomes almost invisible below $0.98T_c$.

The results for the two samples look distinctly different, but if the unknown value of $\lambda(0)$ of sample A were increased relative to the one for sample B, the difference would be greatly diminished. The effect of the T^3 term in the inelastic-scattering rate is clearly visible in this plot. Comparing this figure with the inset of Fig. 7(b), it seems as if the ‘‘fluctuation contribution’’ to $\lambda^2(0)/\lambda^2(T)$ is larger for sample B. However, if T_c for sample A is reduced by 1.1 K to 90.5 K (same as sample B), as has been done to draw this figure, the deviations from the mean-field results become rather similar. Replotting the data as $\lambda^3(0)/\lambda^3(T)$ (inset: solid symbols) gives nearly linear curves, especially for sample B, as one might expect from fluctuation theory.[119] Clearly, T_c needs to be treated as fit parameter when the theory is generalized to include fluctuations[117–119] and inhomogeneities.[119–121]

Figure 13 shows that a good fit to the surface resistance can be obtained. Here, the fit around 35 K is improved by keeping a T^3 contribution to $\Gamma^{\text{inel}}(T)$. The difference between theory and experiment is well within experimental error, though (see Table II). Near T_c the discrepancy between theory and experiment is more noticeable than for sample A, probably due to the smaller transition width $\Delta T_c=0.4$ K (lower left inset). Much of the discrepancy between theory and the data taken with the TE_{013} mode could be removed by choosing T_c somewhat higher than the value measured inductively. Conversely, reducing T_c for sample A would create a very similar discrepancy, as has been discussed above in connection with the superfluid density. The data points above 89 K clearly indicate, though, that the drop in R_s is much steeper for sample B. The order-parameter amplitude for sample B has already been increased by 10% compared to the one for sample A, but this is not enough to produce such a steep drop. Further increases in $\Delta_0(0)$ would lead to a deterioration of the fit at lower temperatures. One possible explanation would be a more rapid rise of $\Delta_0(T)$ below T_c than predicted by weak coupling, with the difference be-

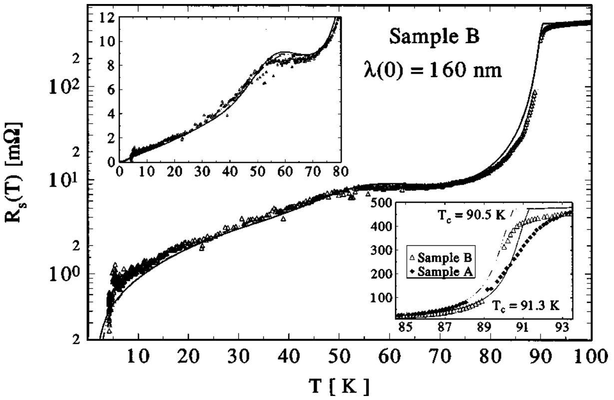

FIG. 13. Surface resistance of sample B obtained from the measured effective surface resistance under the assumption $\lambda(0) = 160$ nm. The coordination between symbols and parameter sets is the same as in Fig. 9. Main frame: semilogarithmic plot; upper left inset: linear plot of R_s at low temperatures; lower right inset: comparison of the two samples in the transition region. Both curves shown are for parameter set B16a with different choices for T_c.

tween the samples attributed to a different spread in T_c's. A semilogarithmic plot of $R_S(T)$ for sample B would show the same change in slope near 86 K as has been found for sample A (see Fig. 8, lower right inset).

B. Scattering rates and the two-fluid model

There has been considerable interest in the scattering rates of quasiparticles at the Fermi surface, even though these quantities cannot be measured directly.[59,92,127] It has been pointed out by Hirschfeld *et al.*[21] that even the elastic-scattering rate $\Gamma = \mathrm{Im}[\omega Z(\omega)]$ obtained from Eq. (23) acquires a strong frequency dependence through renormalization. For a superconductor with isotropic energy gap this frequency dependence cancels in the calculation of the conductivity which then depends only on the normal-state scattering rate Γ_N^{el}. For anisotropic superconductors the situation is more complex.

In Fig. 14 we show scattering rates for sample A at the experimental frequency 87 GHz for parameter sets A16b and A16c used in Figs. 6–8 (full curves, dashed curve). The figure shows that the scattering phase shift has quite a dramatic effect on the scattering rate with both results shown well below the limiting value 2.146 meV which can be obtained to a very good approximation from the self-consistent form of Eq. (37). When the iterated form is used, the γ value obtained is $\approx 10\%$ higher. The change due to our finite frequency is less than 0.5%. The scattering rate depends even more strongly on δ_N than the conductivity (cf. Fig. 4). Comparison between Eqs. (37) and (34) shows that there is no simple relationship between the two quantities. In particular, such a relationship cannot be of the form Eq. (39) because both $\sigma_1(T=0,\omega)$ and $\Gamma(T=0,\omega)$ increase with δ_N due to the effect that scattering has on the density of states and hence on the normal fluid density Eq. (42).

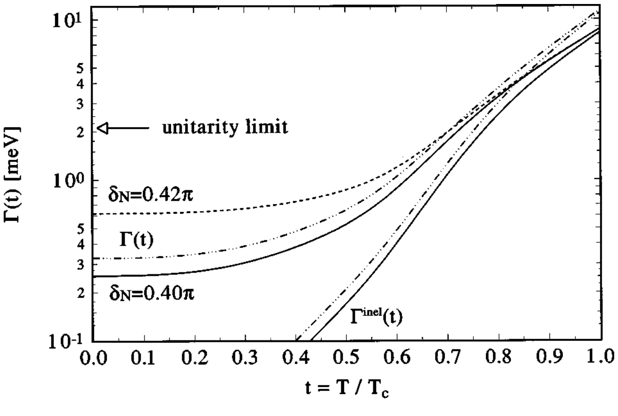

FIG. 14. Total scattering rates and inelastic-scattering rates as function of reduced temperature for sample A at the experimental frequency $f = 87$ GHz. Solid line: A16b; dashed line: A16c; dot-dot-dashed line: A14a.

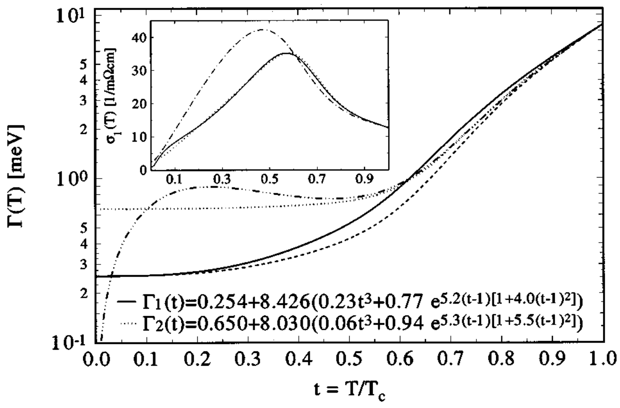

FIG. 15. Phenomenological scattering rates with finite zero-temperature limit. Solid line is identical to the solid line in Fig. 14. $\Gamma_1(t)$ is an excellent fit to the numerical result. The conductivity obtained with this frequency-independent scattering rate is shown in the inset as a dot dashed line. The solid line in the inset is identical with the solid line in Fig. 6, which represented a good fit to the data. The conductivity obtained with $\Gamma_2(t)$ (dotted line) thus also fits the data reasonably well. $\Gamma_2(t)$ is much closer to the frequency averaged scattering rate (dot-dot-dashed line: A16b) than the scattering rate $\Gamma_1(t)$at 87 GHz. For an explanation of the short dashed curve see text.

Also included in the figure are results (dot-dot-dashed) for parameter set A14a with the same phase shift as the solid curve but with a smaller order-parameter amplitude. According to Eq. (37), the zero-temperature zero-frequency-scattering rate increases with $\Delta_0(0)$ in the unitarity limit but decreases with $\Delta_0(0)$ in the Born limit for $\Gamma_N^{\mathrm{el}} \ll \Delta_0(0)$. According to Hirschfeld *et al.*[21] [Eq. (20)] the same behavior is expected at finite frequencies. The fact that the result for $\Delta_0(0) = 3.0 k_B T_c$ (dot-dot-dashed) lies above the one for $\Delta_0(0) = 3.4 k_B T_c$ indicates that at $\delta_N = 0.40\pi$ we are closer to the Born limit than to the unitarity limit.

The parameter sets A14a and A16b also differ in the choice of λ_p which, however, does not explicitly enter the calculation of Γ. As has been discussed above, though, the phenomenological scattering rate $\Gamma^{\mathrm{inel}}(t)$ Eq. (48) has to be modified in order to fit σ_1 for different choices of λ_p. The difference between the solid and the dot-dot-dashed curves demonstrates the sensitivity of $\Gamma^{\mathrm{inel}}(t)$ to the choice of $\lambda(0)$.

With the help of Fig. 15 we shall try to elucidate the relation between the present theory and the two-fluid model.[19,104–106] The solid curve is the same as in Fig. 14 (parameter set A16b). The function $\Gamma_1(t)$ given in the inset is an excellent fit of the form Eq. (48) to the numerical result. Included in the figure as a dashed curve is the function $\Gamma^{\mathrm{inel}}(t)+\Gamma(0)$ with parameters in Γ^{inel} from set A16b and with $\Gamma^{\mathrm{inel}}(T_c)$ adjusted so that the total scattering rate at T_c is unchanged. The difference between these two curves indicates the temperature dependence of the elastic scattering which, according to Eq. (23), is due to the temperature dependence of the order-parameter amplitude Eqs. (18),(19) as well as the temperature dependence of Γ^{inel} which, because of the self-consistency implied in Eq. (23), enters $\Gamma(T)$ not only additively.

The self-consistent calculation of the self-energy according to Eqs. (23),(24),(25) is rather time consuming and one might wonder whether this exercise is actually necessary. To check this point we calculated $\sigma_1(\omega)$ using $\Omega Z(\Omega_\pm)=\Omega \pm i\Gamma_1(t)$. The result (dash dot curve) is compared in the inset with the results of the full calculation (solid curve, identical with the solid curve in Fig. 6). The significant discrepancy has several sources: The approximation used ignores the complex energy shift χ altogether, it neglects corrections to the real part of Z and, most importantly, it neglects the frequency dependence of Z. Exactly the same simplifying assumptions led us to the two-fluid model Eq. (41). Nonetheless, in view of the fact that some functional relationship between $\sigma_1(T,\omega)$ and $\Gamma(T)$ exists, we would expect that for any experimental frequency we can find a scattering rate that would fit the observed conductivity. This is indeed the case, as the dotted curve shown in the inset of Fig. 15, which has been obtained with $\Gamma_2(t)$, demonstrates.

The discrepancy between Γ_1 and Γ_2 is significant only when the frequency-dependent renormalized elastic scattering dominates. This suggests that a more appropriate choice for an effective temperature-dependent scattering rate would be the frequency averaged quantity defined in Eq. (46). $\langle \Gamma^{-1}(T,\Omega)\rangle^{-1}$ is shown in Fig. 15 as a dot-dot-dashed curve. It does indeed agree with Γ_2 over a wide temperature range. The sharp drop at low temperatures is not to be taken seriously because there the condition $\hbar\omega/2k_BT_c=0.023\ll t$, which allowed us to replace $\Gamma(\Omega+\omega)+\Gamma(\Omega)$ by $2\Gamma(\Omega)$, is no longer fulfilled. One would expect the correct low-temperature limit to be $0.5\Gamma(t=0,\omega/2\pi=87\ \mathrm{GHz})$.

In the presence of frequency-dependent self-energy corrections, $1-\rho_n=\rho_s$ no longer holds, so that we cannot determine $\langle \Gamma^{-1}(T,\Omega)\rangle^{-1}$ Eq. (46) from measurements of σ_1 according to Eq. (45) with great accuracy. In the case of elastic scattering, $d\tilde{\Omega}/d\Omega$ is significantly different from 1 only for $\Omega<\Gamma_N^{\mathrm{el}}(t=0,\Omega)$ and $T<\Gamma_N^{\mathrm{el}}$. This is the regime where the dot-dot-dashed curve in Fig. 15 shows strong variations. Since in high-quality samples $\Gamma_N^{\mathrm{el}}\ll T_c$, the difference between ρ_s and $1-\rho_n$ would be negligible at most temperatures. If the frequency dependence of the inelastic scattering is taken into account, the discrepancy between ρ_s and $1-\rho_n$ will be magnified considerably and it will extend over the whole temperature range up to T_c. This is well known from strong-coupling calculations where $d\tilde{\Omega}/d\Omega|_{\Omega=0}=1+\lambda$ is the electron-phonon mass enhancement factor, which renormalizes the London penetration depth,[109] but not $\sigma_1(\omega=0)$ or ρ_n.

Scattering rates for sample B will be presented in Fig. 19 below, together with results from the NFL model.

C. The nested Fermi-liquid model

Consideration of the frequency averaged scattering rate in the previous subsection has demonstrated the importance of the frequency dependence of the elastic-scattering rate resulting from many-body corrections. It would be most desirable to have a similar microscopic model to furnish us with a deeper understanding of the inelastic scattering.[59,92,127] The nested Fermi-liquid (NFL) model described in the previous section[60] provides a description for the inelastic scattering in HTC materials which, in spite of the approximations involved in the derivation of Eq. (29), appears to reflect the essential features of the underlying physical processes.

In Figs. 16 the same experimental results are shown as in Figs. 6–8, but now compared with the results of the NFL model. The parameters g and λ_p are determined from a fit to the normal-state data and the requirement $\lambda(0)=160$ nm (cf. Table IV). The only adjustable parameters left are those characterizing elastic scattering and the order-parameter amplitude. Since the effect of the scattering phase shift has been discussed extensively, we keep δ_N fixed at the value 0.40π which gave the best fit in Figs. 6–8. To reproduce the peak height of $\sigma_1(T)$, Γ_N^{el} had to be reduced. Parameter sets ANFL1 and ANFL2 (Table IV) show the effect of reducing Γ_N^{el}. The order-parameter amplitude is the same as in Figs. 6–8. Comparison of results for parameter sets ANFL2 and ANFL3 shows the effect of reducing the order-parameter amplitude while keeping Γ_N^{el} fixed. The NFL model does yield a peak in σ_1 but the details of the temperature dependence are not very accurately reproduced. Panel (b) shows the ''superfluid density'' and in the inset the change in penetration depth at intermediate and low temperatures. Clearly, the smaller order-parameter amplitude gives the better fit, whereas the exact value of Γ_N^{el} is rather unimportant. The abrupt change in slope around 50 K apparently cannot be explained within the NFL model. It should be noted, though, that the discrepancy is only just outside the experimental error of 5 nm. Panel (c) shows that parameter set ANFL3 gives a good fit to the surface resistance over the whole temperature range. The order-parameter amplitude $2\Delta_0(0)/kT_c=6.8$ used in Figs. 6–8 now gives too steep a drop near T_c. The decrease in R_s with increasing Γ_N^{el} at intermediate temperatures[19,26] is clearly visible.

In Fig. 17 we compare data for sample B and the choice $\lambda(0)=160$ nm with predictions of the NFL model. The only parameter g in this model is somewhat smaller than for sample A because of the difference in normal-state resistivities. To get anywhere near the height of the peak in $\sigma_1(T)$ we had to reduce$2\Delta_0(0)/kT_c$ from 7.4 (B16a, B16b in Figs. 9, 12, 13) to 6.4. To change the height of the calculated peaks we varied Γ_N^{el}. $\Gamma_N^{\mathrm{el}}=0$ gives the highest peak, as expected, but completely disagrees with the data taken below 35 K (cf. inset Fig. 9). Increasing Γ_N^{el} to the range of values used previously for this sample gives a marked improvement in the agreement between theory and experiment at low temperatures without drastically reducing the peak height. Panels (b) and (c) show calculations of the superfluid density and the surface resistance for the same set of parameters, set

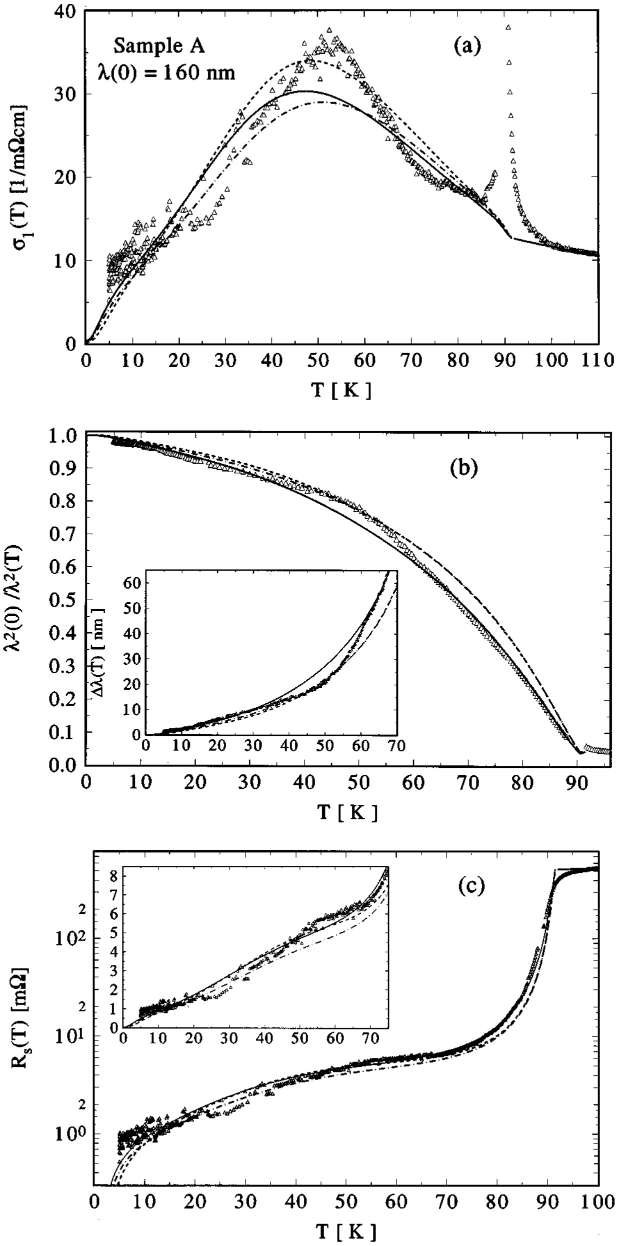

FIG. 16. Comparison of experimental data for sample A with results from the nested Fermi-liquid model. Dashed line: ANFL1 [$\Gamma_N^{\mathrm{el}}=0.15$ meV, $2\Delta_0(0)/kT_c=6.8$]; dot dashed line: ANFL2 [$\Gamma_N^{\mathrm{el}}=0.25$ meV, $2\Delta_0(0)/kT_c=6.8$]; solid line: ANFL3 [$\Gamma_N^{\mathrm{el}}=0.25$ meV, $2\Delta_0(0)/kT_c=6.0$]. Parameter sets given in Table IV. Panel (a): real part of the conductivity. Panel (b): superfluid density and penetration depth. Panel (c): surface resistance.

against the data points already presented in Figs. 11, 12, and 13. In contrast to Fig. 16 the drop in R_s or the rise in $\lambda^2(0)/\lambda^2(T)$ is not fast enough. So, choosing $\Delta_0(0)$ even smaller to increase the height of the peak in σ_1 is not an option. Agreement could be improved by taking T_c about 1.5 K higher than the value measured inductively (cf. discussion of Fig. 13). Apart from this problem near T_c, parameter set BNFL2 fits R_s rather well for all temperatures. The shoulder at 55 K is better reproduced using $\Gamma_N^{\mathrm{el}}=0$ but this choice leads to distinct disagreement with the data taken at lower temperatures. The low-temperature behavior of $\lambda^2(0)/\lambda^2(T)$ at this finite frequency is also better explained assuming a finite elastic-scattering rate. The change in slope around 50 K, which is much more pronounced for sample B than for sample A, cannot be accounted for within this NFL model.

TABLE IV. Parameter sets used to generate theoretical fits based on the nested Fermi-liquid model for the inelastic scattering.

Parameter set	Γ_N^{el} [meV]	δ_N	g	$\frac{2\Delta_0(0)}{kT_c}$	λ_p [nm]	$\lambda(0)$ [nm]
ANFL1	0.15	0.40π	0.624	6.8	175.3	155.91
ANFL2	0.25	0.40π	0.625	6.8	173.8	159.64
ANFL3	0.25	0.40π	0.625	6.0	173.8	160.02
BNFL1	0.00		0.583	6.4	175.4	160.07
BNFL2	0.05	0.44π	0.584	6.4	174.2	159.91
BNFL3	0.11	0.44π	0.585	6.4	173.1	160.03

In order to gain a better understanding of the difference between the NFL model and the purely phenomenological model Eq. (47) we display in Fig. 18 the inelastic-scattering rates which are embedded in the theoretical results shown in Figs. 6–8 and 16. Also shown are the total scattering rates at $f=87$ GHz and the frequency averaged scattering rates Eq. (46). Over several orders of magnitude $\Gamma_{\mathrm{NFL}}^{\mathrm{inel}}(87\ \mathrm{GHz},T)$ (dot-dot-dashed line) varies as T^3 [cf. Eq. (32)]. The magnitude of this cubic term agrees well with that deduced from the fit (long dashed line, A16b). Because of the finite frequency considered, $\Gamma_{\mathrm{NFL}}^{\mathrm{inel}}$ approaches a finite value for $T\rightarrow 0$ [cf. Eq. (33)]. The frequency averaged scattering rate for parameter set A16b (Table III) with δ_N changed to $\pi/2$ (alt. dashed line) goes through a minimum before reaching a relative maximum at $t=0$. For intermediate scattering phase shifts the minimum is much less pronounced and may be absent altogether.[21,92,128]

At small frequencies we have from Eq. (29) $\Gamma_{\mathrm{NFL}}^{\mathrm{inel}}(T_c)=1.793g^2T_c=5.52$ meV which is smaller than $\Gamma^{\mathrm{inel}}(T_c)=8.25$ meV (A16b), partly because we are using in the NFL model a larger value of λ_p but the same value of $\sigma_1(T_c)$, and partly because the calculation of σ_1 from Eq. (38) at high temperatures involves $\Gamma_{\mathrm{NFL}}^{\mathrm{inel}}(\Omega,T)$ with $\Omega\gg\omega$. The frequency averaged NFL scattering rate at T_c (inset, dotted line) is 6.87 meV. Extrapolating the cubic low-temperature behavior Eq. (32) to T_c we would have $\Gamma_{\mathrm{NFL}}^{\mathrm{inel}}(T_c)=3.681\ [kT_c/\Delta_0(0)]^2g^2T_c=0.409g^2T_c$. Since this value is smaller than the one obtained at T_c, $\Gamma_{\mathrm{NFL}}^{\mathrm{inel}}$ must drop faster than T^3 near T_c. The inset (dot-dot-dashed line) shows that this decrease is exponential. The size of this exponential drop gets larger when the order parameter amplitude is increased, as the alt. dashed line in the inset shows. For this reason, $\sigma_1(T)$ rises more slowly below T_c when a smaller value for $\Delta_0(0)$ is chosen, as is seen in Fig. 16 [panel (a)]. The most important difference between $\Gamma_{\mathrm{NFL}}^{\mathrm{inel}}(\Omega,T)$ and $\Gamma^{\mathrm{inel}}(T)$ occurs at temperatures 50 K $<T<$ 85 K, where Γ^{inel} shows a much more rapid drop, produced by the correction term in the exponent in Eq. (48). This behavior still remains to be understood.

In Fig. 19 we compare scattering rates for sample B resulting from the two parameter sets used in Fig. 9 for

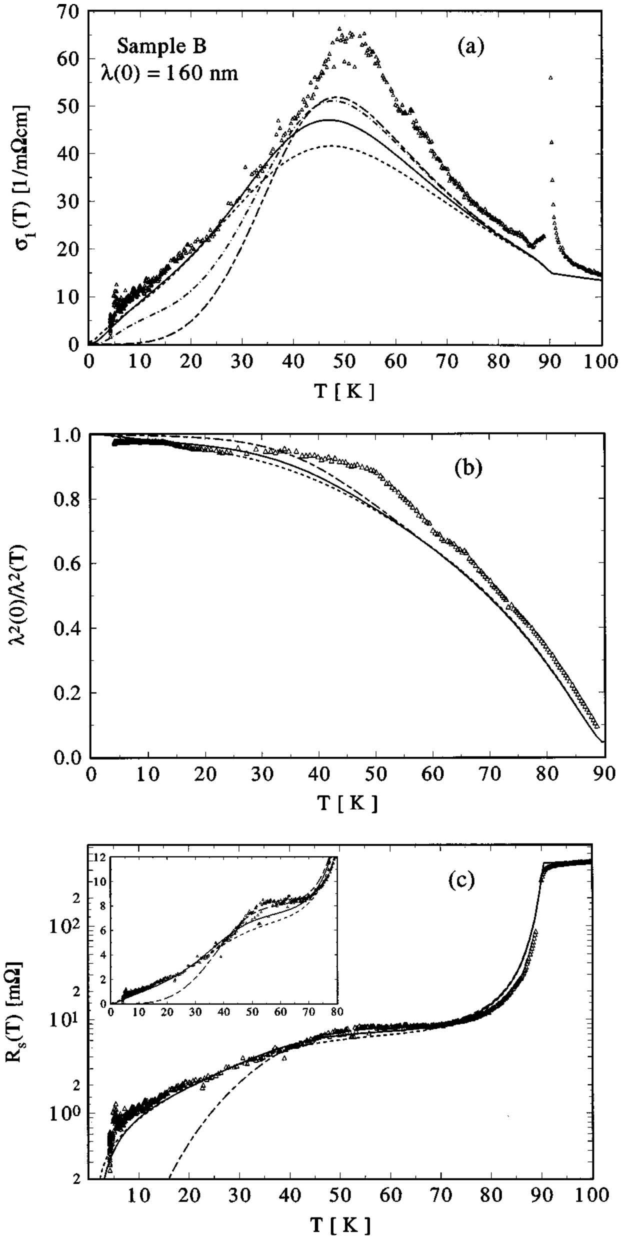

FIG. 17. Comparison of experimental data for sample B with results from the nested Fermi-liquid model. Alt. dashed line: BNFL1 ($\Gamma_N^{\mathrm{el}}=0.00$ meV); dot dashed line: ($\Gamma_N^{\mathrm{el}}=0.01$ meV); solid line: BNFL2 ($\Gamma_N^{\mathrm{el}}=0.05$ meV); dashed line: BNFL3 ($\Gamma_N^{\mathrm{el}}=0.11$ meV).

$\lambda(0)=160$ nm and from parameter set BNFL2 (Table IV), which gave the best fit within the NFL model in Fig. 17. The total scattering rates $\Gamma(0)$ come out differently because of differences in scattering phase shifts and elastic-scattering rates. Clearly, $\Gamma(0)$ is more sensitive to changes in δ_N than to changes in Γ_N^{el}. The long dashed line represents the frequency averaged scattering rate in the unitarity limit. In this semilogarithmic plot the minimum already discussed in connection with Fig. 18 is much more noticeable. The different low-temperature limits of the total scattering rates at 87 GHz is reflected in the low-temperature behavior of the frequency averaged scattering rates. But these sizable variations in the scattering rates at around $0.1T_c$ have comparatively little effect on R_s or $\Delta\lambda$.

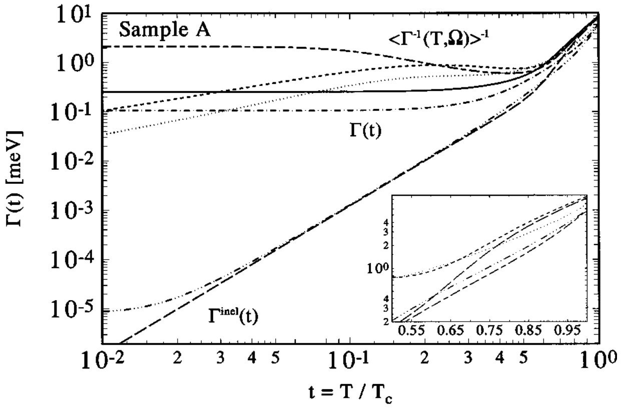

FIG. 18. Comparison of scattering rates deduced from fits to experimental data on sample A with results from the NFL model. Dot dashed, dot-dot-dashed, and dotted lines: NFL model (ANFL3, Table IV). Solid, long dashed, and short dashed lines: (A16b, Table III). The alt. dashed line represents the frequency averaged scattering rate in the unitarity limit $\delta_N=\pi/2$. The alt. dashed line in the inset is an NFL result for an increased order parameter amplitude (ANFL2).

The inelastic-scattering rates differ greatly, primarily because of the presence of a t^3 term in one of the parameter sets. While this difference affects primarily the behavior at low temperatures, where elastic scattering dominates, there is a significant change in the frequency averaged scattering rate around $t=0.4$ which can be viewed as the physical origin of the marked difference in $\Delta\lambda(T)$ calculated for the two parameter sets and shown in Figs. 11 and 12. Closer to T_c the t^3 term is balanced by a more rapid exponential decrease (increased values of b_1 and b_2). Within the NFL model there is always a t^3 contribution to the scattering rate unless the phase space for spin fluctuation exchange decreases more rapidly in the superconducting state than the density of states Eq. (30).

It is remarkable that within this NFL model we had to assume λ_p larger than $\lambda(0)$. The downward renormalization

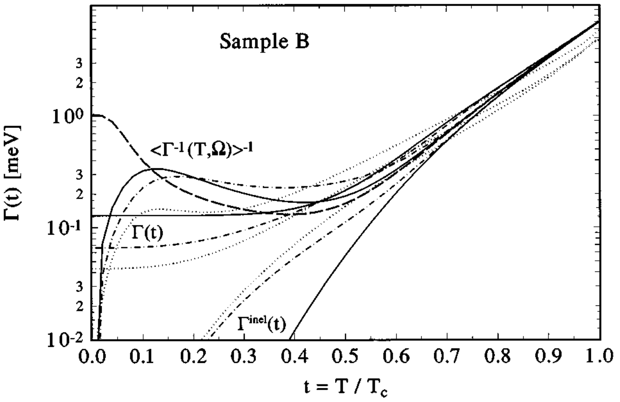

FIG. 19. Comparison of scattering rates deduced from fits to experimental data on sample B with results from the NFL model. Dotted lines: BNFL2, Table IV, solid lines: B16a, Table III, dot dashed lines: B16b, Table III. The long dashed line represents the frequency averaged scattering rate in the unitarity limit. Other parameters are from the set B16a. This figure elucidates the role of the T^3 term in the inelastic-scattering rate.

of the plasma wavelength resulting from the frequency dependence of $\Gamma_{\mathrm{NFL}}^{\mathrm{inel}}$ appears to be responsible for the fact that we can fit the steep drop in R_s and $\lambda(T)$ with smaller order-parameter amplitudes (cf. Tables III and IV). When the real part of the self-energy due to spin fluctuation exchange is included we find the large upward renormalization of λ_p known from strong-coupling calculations.[109] In this case the two parameters g and λ_p at our disposal are not sufficient to fit the normal-state resistivity measured by ourselves as well as the London penetration depth $\lambda(0)$ which is restricted to lie in a rather narrow range by other experiments.[30–35]

This failure of the NFL model should not be too surprising in view of the approximations involved. Using the random phase approximation appears to be one necessary step to generalize the theory. Another shortcoming, not so easily remedied, is the crude treatment of the momentum dependence of the self-energy: the spin susceptibility is taken at the nesting vector, which simplifies the final expression, but otherwise the momentum dependence is completely neglected. If one goes to the length of taking the frequency dependence fully into account, one should then also consider the frequency dependence in more detail by doing a strong-coupling calculation. This is the approach taken in the fluctuation-exchange approximation (FLEX),[44] for which no such detailed calculations of the conductivity including elastic scattering have yet been published. It is also an open question whether the degrees of freedom responsible for the formation of the superconducting state are exactly the same as those determining the transport properties.

We still believe that the scattering rate as calculated in the NFL model does reflect important intrinsic properties of high-temperature superconductors.

V. CONCLUSIONS

Both the surface resistance and the change in the penetration depth measured at 87 GHz on one electron-beam evaporated (sample A) and one high oxygen pressure dc sputtered (sample B) YBCO film, optimized for low-rf losses, have been interpreted successfully in the whole temperature range in terms of a d-wave model of superconductivity. There was no need to subtract some extrinsic residual surface resistance. This leads us to the conclusion that such a d-wave model does indeed reflect the most important intrinsic features of the superconducting state in high-T_c materials.

Essential for the success of the theory is the use of an elastic s-wave scattering rate rather larger than has been used elsewhere[21] but small enough to have negligible effect on T_c, and an intermediate scattering phase shift. The resulting quasiparticle mean-free paths at $T=0$ are larger than the distance between twin boundaries, but they do not appear unreasonably long. While both weak- and strong-scattering limits lead to quadratic temperature dependences in both $\Delta\lambda(T)$ and $R_s(T)$, intermediate-scattering phase shifts can account for the observed quasilinear behavior up to around $T_c/2$. The self-energy part χ, which renormalizes the quasiparticle energy and which is relevant only at intermediate-scattering phase shifts, has only a rather limited effect on the conductivity at our measuring frequency. At lower frequencies it is absolutely essential to take χ into account in order to retain the quasilinear temperature variation of $\sigma_1(T)$.

There is considerable variation between the two samples investigated. This can be attributed primarily to a difference in the elastic-scattering rates which seems plausible in view of the different structural properties of the samples. The sensitivity to these scattering rates is related to the fact that they are comparable to the external frequency.

The actual symmetry of the order parameter cannot be tested by this type of experiment. An s-wave state with twice as many nodal lines can give identical results. To be compatible with the data, the pair states should have nearly vanishing Fermi surface averages so that their momentum dependences are not significantly modified by elastic scattering. In that case, the complex conductivity becomes very sensitive to the scattering phase shift. An s-wave order parameter which has, in the clean limit, exactly the same density of states as the d-wave state considered can be excluded, because for this state elastic scattering is close to the weak-scattering limit for any value of the scattering phase shift so that the large conductivity observed at low temperatures cannot be accounted for. The difference in the strength of scattering is also reflected in changes of the density of states at very low energies.[50,52] For the small elastic-scattering rates required to fit our data, changes in the density of states are far too small to be detected in other experiments such as ARPES or tunneling. States with a finite minimum energy gap give results very similar to those of the above s-wave state when the broadening of the density of states at finite temperatures due to strong-coupling effects is taken into account.[18]

The conclusions so far are based on the comparison between theory and experiment in the temperature range between 4.2 K and $\approx T_c/2$, where extrinsic losses might dominate. Due to the use of a copper cavity, which permitted measurements on rather large films at high frequency, our measuring sensitivity becomes low at very low temperatures. A more stringent test of the theory would require data taken with high resolution at even lower temperatures.

At intermediate temperatures and close to T_c the most important aspect of this theory is a temperature-dependent scattering rate resulting from inelastic interactions. This phenomenological scattering rate can be adjusted to fit the conductivity for a wide range of pair states excluding only those with a large, nearly isotropic energy gap. The part of the data which is most likely to reflect intrinsic properties, therefore, does not provide the salient information that would allow us to distinguish between different pair states.

Within the d-wave model used here, parameters can be found that lead to an excellent fit for the real part σ_1 of the conductivity, but fail to provide a reasonable fit to R_s and $\Delta\lambda$. In particular, large peaks in $\sigma_1(T)$ and large residual losses are most easily explained in terms of small order parameter amplitudes $\Delta_0(0)$, but these would be incompatible with the sharp drop of both R_s and $\Delta\lambda$ at T_c. The fact that $\Delta_0(0)$ is estimated to be $\approx 10\%$ larger for sample B than for sample A is related to the difference in transition widths. All our estimates for $\Delta_0(0)$ are considerably larger than the weak-coupling value but are well within generally accepted estimates. A different choice of the temperature-dependent scattering rate does not solve the problem because when $\Gamma(T)$ is made to decrease faster below T_c, $\lambda(T)$ will also decrease somewhat faster but σ_1 will increase and as a result R_s will generally drop less precipitously.

A smaller order parameter amplitude could be arrived at if $\Delta_0(T)$ were to rise faster than predicted by weak-coupling theory. It does not seem feasible to study this effect in the present context at the expense of introducing even more parameters, because the R_s data above T_c clearly show the importance of fluctuations. These can be expected to affect the electromagnetic response below T_c as well. The importance of the fluctuations was only recognized because our data extended well into the normal state. If we had not included these data in our mean-field analysis, the data taken in the superconducting state could all have been fitted very well simply by changing some of the parameters, resulting in some erroneous conclusions.

An order parameter whose average over the Fermi surface vanishes or is, at any rate, very small, is a consequence of the strong on-site repulsion of quasiparticles which is believed to be one of the most important characteristics of high-T_c materials.[41] The kind of d-wave state considered here would follow rather naturally from the exchange of antiferromagnetic spin fluctuations. The same interaction would give a temperature (and frequency) dependent scattering rate.

Using the nested Fermi-liquid model[60] we find that $\Gamma^{\mathrm{inel}}(T)$ at low frequencies can be approximated by the sum of an exponentially decreasing term and a contribution varying as T^3. This is very similar to the phenomenological scattering rate derived from fitting the data for sample A, except that the exponential decrease of $\Gamma^{\mathrm{inel}}_{\mathrm{NFL}}(T)$ is not quite fast enough to provide an equally good fit. For sample B the fit especially to $\Delta\lambda(T)$ is not quite so satisfactory because of the T^3 contribution. It is not clear why this contribution should be present in one sample and not in the other. Note, that only a prefactor in $\Gamma^{\mathrm{inel}}_{\mathrm{NFL}}(T)$ is changed from one sample to the other to account for the difference in the normal-state resistivity ρ_n. The comparison between microscopic scattering rates and those derived from experiments using, for example, a fit procedure as in this paper or a two-fluid model is not straightforward because the ‘‘measured’’ scattering rates always involve an average over frequency with a temperature-dependent weighting factor.

VI. FURTHER WORK

In order to further substantiate the argument that the surface impedance in these films is indeed dominated by intrinsic effects, even at low temperatures, a detailed comparison with data for twinned and untwinned crystals would be desirable. A somewhat preliminary study has shown that the surface resistance measured on twinned single crystals at 10.1 GHz (Ref. 27) and 9.6 GHz (Ref. 20) seems to be consistent with this theory. Because of sample differences the parameters entering the calculation are, of course, different. Similarly, the 4.13 GHz data of the UBC group[19,26,28] for both the twinned and the untwinned crystal can be fitted using a smaller elastic-scattering rate for the untwinned crystal. For both crystals the elastic scattering rates giving optimal fits are smaller than those required to fit the thin film data. This is consistent with the picture of twin boundaries, which in crystals are more widely spaced than in films, contributing to the disorder-induced scattering. At 34.8 GHz the surface resistance of the twinned crystal[28] is too high to be compatible with this theory. For the detwinned crystal[26] good agreement between theory and experiment can be achieved with the same parameters that were used to fit the low-frequency data, except at low temperatures. There, the calculated R_s values are lower than the data points while at the lower frequency the data points for the untwinned crystal are below the theoretical values. Hence, there seems to be no parameter set that would fit the data at both frequencies with the same accuracy that we were able to achieve with our 87 GHz thin film data. More experiments designed to reveal the frequency dependence at low temperatures (cf. Fig. 10) would be needed to provide a more stringent test for this theory.

Near the transition temperature fluctuations clearly make an important contribution so that the present theory needs to be generalized to describe fluctuations in a consistent manner. Since it is our conviction that conclusions are greatly strengthened when drawn from a comparison between theory and both real and imaginary part of the conductivity, we did not include a discussion of fluctuation effects in the present paper, because we are not able to measure the shift in penetration depth above 88 K.

The most serious objection that can be raised against the theory presented here is the size of the normal-scattering rate derived from the resistivity, which would suffice to suppress the transition to a d-wave state or any other highly anisotropic state in a weak-coupling calculation. To answer this criticism one needs to do a strong-coupling calculation. This would require a generalized momentum-dependent Eliashberg function, calculated self-consistently in the superconducting state as, for example, in the FLEX approximation.[44] Including a pairing interaction that peaks at small momentum transfer[48] would certainly allow to fit T_c and ρ_n simultaneously but at the same time it would render the theory even more complex. Furthermore, as we have shown here, any such theory would be incapable of describing the electromagnetic response over much of the temperature range below T_c unless a small but unavoidable amount of elastic scattering is taken into account. If such a calculation were possible, anisotropy of the quasiparticle velocities and quasiparticle scattering rates would be included at no extra cost.

Another important problem presently under investigation by several groups is the relationship between the ab-plane response studied here and the c-axis conductivity. Attributing the observed c-axis conductivity solely to incoherent scattering[129] is inconsistent with the small amount of elastic s-wave scattering derived here. If scattering between planes very nearly conserves the in-plane momentum, then p- and d-wave scattering would have to be considered requiring the evaluation of vertex corrections with respect to impurity scattering.

ACKNOWLEDGMENTS

We thank R. G. Humphreys, N. G. Chew, and J. A. Edwards from DRA Malvern, UK, for providing the evaporated YBCO film and performing the x-ray analyses and M. Lenkens, M. Getta, and R. Wagner from University of Wuppertal, Germany, for providing the sputtered YBCO film and performing the inductive measurements. We are much obliged to D. A. Bonn, W. N. Hardy, T. Jacobs, S. Sridhar, and S. M. Anlage for discussions on the work done on single crystals and for making their data available to us in electronic form. One of the authors (C.T.R.) gratefully acknowledges discussions with J. Ruvalds on the nested Fermi-liquid model. This work has been funded in part by the CEC-ESPRIT Basic Research Project 6113 and by the Deutsche Forschungsgemeinschaft through the Graduiertenkolleg ‘‘Physik nanostrukturierter Festkörper.’’

---

[1] N. Klein, G. Müller, H. Piel, B. Roas, L. Schultz, U. Klein, and M. Peiniger, Appl. Phys. Lett. **54**, 757 (1989).

[2] L. Drabeck, G. Grüner, J. J. Chang, A. Inam, X. D. Wu, L. Nazar, T. Venkatesan, and D. J. Scalapino, Phys. Rev. B **40**, 7350 (1989).

[3] G. Müller, N. Klein, A. Brust, H. Chaloupka, M. Hein, S. Orbach, H. Piel, and D. Reschke, J. Supercond. **3**, 235 (1990).

[4] N. G. Chew, J. A. Edwards, R. G. Humphreys, J. S. Satchell, S. W. Goodyear, B. Dew, N. J. Exon, S. Hensen, M. Lenkens, G. Müller, and S. Orbach-Werbig, IEEE Trans. Appl. Supercond. **5**, 1167 (1995); R. G. Humphreys (private communication).

[5] B. Avenhaus, A. Porch, M. J. Lancaster, S. Hensen, M. Lenkens, S. Orbach-Werbig, G. Müller, U. Dähne, N. Tellmann, N. Klein, C. Dubourdieu, O. Thomas, H. Karl, B. Stritzker, J. A. Edwards, and R. G. Humphreys, IEEE Trans. Appl. Supercond. **5**, 1737 (1995).

[6] S. Hensen, M. Lenkens, M. Getta, G. Müller, B. Avenhaus, A. Porch, and M. J. Lancaster, in *Applied Superconductivity 1995*, edited by D. Dew-Hughes (IOP, Bristol, 1995), Vol. 2, p. 1127.

[7] W. Diete, M. Getta, M. Hein, T. Kaiser, G. Müller, H. Piel, and H. Schlick, IEEE Trans. Appl. Supercond. (to be published).

[8] H. Piel and G. Müller, IEEE Trans. Magn. **MAG-27**, 854 (1991).

[9] P. Nguyen, D. Oates, G. Dresselhaus, and M. Dresselhaus, Phys. Rev. B **48**, 6400 (1993).

[10] G. Dionne, IEEE Trans. Appl. Supercond. **3**, 1465 (1993).

[11] S. Sridhar, D.-H. Wu, and W. Kennedy, Phys. Rev. Lett. **63**, 1873 (1989).

[12] J. Halbritter, J. Supercond. **8**, 691 (1995).

[13] N. Klein, N. Tellmann, H. Schulz, K. Urban, S. A. Wolf, and V. Z. Kresin, Phys. Rev. Lett. **71**, 3355 (1993).

[14] S. Orbach-Werbig, A. Golubov, S. Hensen, G. Müller, and H. Piel, Physica C **235-240**, 1823 (1994).

[15] V. Kresin and S. Wolf, Phys. Rev. B **51**, 1229 (1995).

[16] V. Z. Kresin, H. Morawitz, and S. A. Wolf, *Mechanisms of Conventional and High* T_c *Superconductivity* (Oxford, New York, 1993).

[17] A. A. Golubov, M. R. Trunin, and A. A. Zhukov, JETP Lett. **62**, 496 (1995).

[18] A. A. Golubov, M. R. Trunin, A. A. Zhukov, O. V. Dolgov, and S. V. Shulga, J. Phys. (France) I **6**, 2275 (1996).

[19] D. A. Bonn, Ruixing Liang, T. M. Riseman, D. J. Baar, D. C. Morgan, Kuan Zhang, P. Dosanjh, T. L. Duty, A. MacFarlane, G. D. Morris, J. H. Brewer, and W. N. Hardy, Phys. Rev. B **47**, 11 314 (1993).

[20] J. Mao, D. H. Wu, J. L. Peng, R. L. Greene, and S. M. Anlage, Phys. Rev. B **51**, 3316 (1995).

[21] P. J. Hirschfeld, W. O. Putikka, and D. J. Scalapino, Phys. Rev. B **50**, 10 250 (1994).

[22] D. Xu, S. K. Yip, and J. A. Sauls, Phys. Rev. B **51**, 16 233 (1995).

[23] D. A. Bonn and W. N. Hardy, in *Physical Properties of High Temperature Superconductors V*, edited by D. M. Ginsberg (World Scientific, Singapore, 1995), Vol. 5, p. 7.

[24] D. A. Bonn, S. Kamal, A. Bonakdarpour, Ruixing Liang, W. N. Hardy, C. C. Homes, D. N. Basov, and T. Timusk, in *Proceedings of the 21st International Conference on Low Temperature Physics* [Czech. J. Phys. **46-S6**, 3195 (1996)].

[25] T. L. Hylton *et al.*, Appl. Phys. Lett. **53**, 343 (1988); T. L. Hylton and M. R. Beasley, Phys. Rev. B **39**, 9042 (1989).

[26] D. A. Bonn, S. Kamal, Kuan Zhang, Ruixing Liang, D. J. Baar, E. Klein, and W. N. Hardy, Phys. Rev. B **50**, 4051 (1994).

[27] T. Jacobs, S. Sridhar, C. T. Rieck, K. Scharnberg, T. Wolf, and J. Halbritter, J. Phys. Chem. Solids **56**, 1945 (1995).

[28] D. A. Bonn, D. C. Morgan, Kuan Zhang, Ruixing Liang, D. J. Baar, and W. N. Hardy, J. Phys. Chem. Solids **54**, 1297 (1993).

[29] Y. Zhu and M. Suenaga, in *Interfaces in High-*T_c *Superconducting Systems*, edited by S. L. Shindé and D. A. Rudman (Springer-Verlag, New York, 1994), p. 140.

[30] J. E. Sonier, R. F. Kiefl, J. H. Brewer, D. A. Bonn, J. F. Carolan, K. H. Chow, P. Dosanjh, W. N. Hardy, Ruixing Liang, W. A. MacFarlane, P. Mendels, G. D. Morris, T. M. Riseman, and J. W. Schneider, Phys. Rev. Lett. **72**, 744 (1994).

[31] D. N. Basov, R. Liang, D. A. Bonn, W. N. Hardy, B. Dabrowski, M. Quijada, D. B. Tanner, J. P. Rice, D. M. Ginsberg, and T. Timusk, Phys. Rev. Lett. **74**, 598 (1995).

[32] A. Porch, M. Lancaster, and R. Humphreys, Physica B **195-196**, 1605 (1994).

[33] U. Dähne, Y. Goncharov, N. Klein, N. Tellmann, G. Kozlov, and K. Urban, J. Supercond. **8**, 129 (1995).

[34] H. Porteanu, K. Karraï, R. Seifert, F. Koch, P. Berberich, and H. Kinder, Phys. Rev. Lett. **75**, 3934 (1995).

[35] L. A. de Vaulchier, J. P. Vieren, Y. Guldner, N. Bontemps, R. Combescot, Y. Lemaître, and J. C. Mage, Europhys. Lett. **33**, 153 (1996).

[36] R. A. Klemm, K. Scharnberg, D. Walker, and C. T. Rieck, Z. Phys. B **72**, 139 (1988).

[37] P. J. Hirschfeld, P. Wölfle, D. Einzel, J. A. Sauls, and W. O. Putikka, Phys. Rev. B **40**, 6695 (1989).

[38] J. F. Annett, N. Goldenfeld, and A. J. Leggett, in *Physical Properties of High Temperature Superconductors V* (Ref. 23), p. 375.

[39] D. A. Wollman, D. J. Van Harlingen, J. Giapintzakis, and D. M. Ginsberg, Phys. Rev. Lett. **74**, 797 (1995); A. Mathai, Y. Gim, R. C. Black, A. Amar, and F. C. Wellstood, *ibid.* **74**, 4523 (1995); Y. Gim, A. Mathai, R. C. Black, A. Amar, and F. C. Wellstood, J. Phys. (France) I **6**, 2299 (1996); D. A. Brawner and H. R. Ott, Phys. Rev. B **50**, 6530 (1994); I. Iguchi and Z. Wen, *ibid.* **49**, 12 388 (1994).

[40] C. C. Tsuei, J. R. Kirtley, C. C. Chi, Lock See Yu-Jahnes, A. Gupta, T. Shaw, J. Z. Sun, and M. B. Ketchen, Phys. Rev. Lett. **73**, 593 (1994); J. R. Kirtley *et al.*, *ibid.* **76**, 1336 (1996); J. R. Kirtley and Chang C. Tsuei, Sci. Am. (Int. Ed.) **275** (2), 50 (1996).

[41] D. J. Scalapino, Phys. Rep. **250**, 329 (1995).

[42] P. Monthoux and D. Pines, Phys. Rev. B **47**, 6069 (1993).

[43] P. Monthoux and D. Pines, Phys. Rev. B **49**, 4261 (1994).

[44] L. Tewordt, J. Low Temp. Phys. **15**, 349 (1974); L. Tewordt, D. Fay, P. Dörre, and D. Einzel, *ibid.* **21**, 645 (1975); N. E. Bickers, D. J. Scalapino, and S. R. White, Phys. Rev. Lett. **62**, 961 (1989); N. E. Bickers and D. J. Scalapino, Ann. Phys. (N.Y.) **193**, 206 (1989); T. Dahm and L. Tewordt, Physica C **246**, 61 (1995); T. Dahm, D. Manske, and L. Tewordt, Phys. Rev. B **54**, 6640 (1996).

[45] J. R. Schrieffer, J. Low Temp. Phys. **99**, 397 (1995).

[46] T. Egami and S. J. L. Billinge, in *Physical Properties of High Temperature Superconductors V* (Ref. 23), p. 265.

[47] O. K. Andersen, S. Y. Savrasov, O. Jepsen, and A. I. Liechtenstein, J. Low Temp. Phys. **105**, 285 (1996).

[48] T. Dahm, J. Erdmenger, K. Scharnberg, and C. T. Rieck, Phys. Rev. B **48**, 3896 (1993).

[49] M. E. Flatté, S. Quinlan, and D. J. Scalapino, Phys. Rev. B **48**, 10 626 (1993).

[50] R. Fehrenbacher and M. R. Norman, Phys. Rev. B **50**, 3495 (1994).

[51] D. S. Hirashima, Phys. Rev. B **50**, 10 142 (1994).

[52] L. S. Borkowski and P. J. Hirschfeld, Phys. Rev. B **49**, 15 404 (1994).

[53] T. P. Devereaux, Phys. Rev. Lett. **74**, 4313 (1995).

[54] P. Chaudhari and S.-Y. Lin, Phys. Rev. Lett. **72**, 1084 (1994); A. G. Sun, D. A. Gajewski, M. B. Maple, and R. C. Dynes, *ibid.* **72**, 2267 (1994); A. G. Sun, A. Truscott, A. S. Katz, R. C. Dynes, B. W. Veal, and C. Gu, Phys. Rev. B **54**, 6734 (1996).

[55] K. A. Kouznetsov, A. G. Sun, B. Chen, A. S. Katz, S. R. Bahcall, J. Clarke, R. C. Dynes, D. A. Gajewski, S. H. Han, M. B. Maple, J. Gianpintzakis, J.-T. Kim, and D. M. Ginsberg, cond-mat/9705283, 1997 (to be published).

[56] P. B. Allen and B. Mitrovic, in *Solid State Physics*, edited by H. Ehrenreich, F. Seitz, and D. Turnbull (Academic, New York, 1982), Vol. 37, p. 1.

[57] P. B. Allen, Phys. Rev. B **3**, 305 (1971).

[58] C. M. Varma, P. B. Littlewood, S. Schmitt-Rink, E. Abrahams, and A. E. Ruckenstein, Phys. Rev. Lett. **63**, 1996 (1989); P. B. Littlewood and C. M. Varma, J. Appl. Phys. **69**, 4979 (1991); Phys. Rev. B **46**, 405 (1992); E. J. Nicol and J. P. Carbotte, *ibid.* **44**, 7741 (1991).

[59] B. W. Statt and A. Griffin, Phys. Rev. B **46**, 3199 (1992).

[60] A. Virosztek and J. Ruvalds, Phys. Rev. B **42**, 4064 (1990); C. T. Rieck, W. A. Little, J. Ruvalds, and A. Virosztek, Solid State Commun. **88**, 395 (1993); Phys. Rev. B **51**, 3772 (1995); J. Ruvalds, Supercond. Sci. Technol. **9**, 905 (1996).

[61] C. T. Rieck and K. Scharnberg (unpublished).

[62] K. Zhang, D. A. Bonn, S. Kamal, Ruixing Liang, D. J. Baar, W. N. Hardy, D. Basov, and T. Timusk, Phys. Rev. Lett. **73**, 2484 (1994).

[63] D. M. Ginsberg, W. C. Lee, and S. E. Stupp, Phys. Rev. B **47**, 12 167 (1993).

[64] D. Wehler, G. Müller, Ch. Murek, H. Piel, K. Schönmann, Th. Wolf, and S. A. Wolf, Physica C **235-240**, 2003 (1994).

[65] W. A. Atkinson and J. P. Carbotte, Phys. Rev. B **52**, 10 601 (1995); W. A. Atkinson, J. P. Carbotte, and C. O'Donovan (unpublished).

[66] C. O'Donovan and J. P. Carbotte, Phys. Rev. B **52**, 4568 (1995); J. Low Temp. Phys. **105**, 495 (1996).

[67] H. Kim and E. J. Nicol, J. Phys. Chem. Solids **56**, 1725 (1995).

[68] S. D. Adrian, M. E. Reeves, S. Wolf, and V. Kresin, Phys. Rev. B **51**, 6800 (1995).

[69] N. Chew, S. W. Goodyear, J. A. Edwards, J. S. Satchell, and R. G. Humphreys, Appl. Phys. Lett. **57**, 2016 (1990).

[70] R. Humphreys, J. S. Satchell, N. G. Chew, J. A. Edwards, S. W. Goodyear, S. E. Blenkinsop, O. D. Dosser, and A. G. Cullis, Supercond. Sci. Technol. **3**, 38 (1990).

[71] M. Lenkens, B. Aschermann, S. Hensen, M. Jeck, S. Orbach, H. Schlick, H. Chaloupka, G. Müller, and H. Piel, J. Alloys Compd. **195**, 559 (1993).

[72] M. Lenkens, B. Aschermann, S. Hensen, S. Orbach-Werbig, H. Schlick, G. Müller, M. J. Lancaster, A. Porch, J. R. Powell, and J. A. Edwards, in *Applied Superconductivity*, edited by H. Freyhardt (DGM Informationsgesellschaft Verlag, Oberursel, Germany, 1993), Vol. 2, p. 1061.

[73] M. Lenkens, Ph.D. thesis, Bergische Universität GH Wuppertal, 1996.

[74] A. Gladun, N. Cherpak, A. Gippius, S. Hensen, M. Lenkens, G. Müller, S. Orbach, and H. Piel, Cryogenics **32**, 1071 (1992).

[75] J. Jorgensen, B. W. Veal, A. P. Paulikas, L. J. Lowicki, G. W. Crabtree, H. Claus, and W. K. Kwok, Phys. Rev. B **41**, 1863 (1990).

[76] C. E. Gough and N. J. Exon, Phys. Rev. B **50**, 488 (1994).

[77] S. Hensen, S. Orbach-Werbig, G. Müller, H. Piel, N. G. Chew, J. A. Edwards, and R. G. Humphreys, in *Applied Superconductivity* (Ref. 72), p. 1053.

[78] G. Reuter and E. Sondheimer, Proc. R. Soc. London, Ser. A **195**, 336 (1948).

[79] N. Klein, H. Chaloupka, G. Müller, S. Orbach, H. Piel, B. Roas, L. Schultz, U. Klein, and M. Peiniger, J. Appl. Phys. **67**, 6940 (1990).

[80] J.-J. Chang and D. J. Scalapino, Phys. Rev. B **40**, 4299 (1989).

[81] C. Zuccaro, C. T. Rieck, and K. Scharnberg, Physica C **235-240**, 1807 (1994).

[82] G. Rickayzen, in *Theory of Superconductivity* (Interscience, New York, 1965), p. 427.

[83] W. Lee, D. Rainer, and W. Zimmermann, Physica C **159**, 535 (1989).

[84] R. Akis and J. P. Carbotte, Solid State Commun. **79**, 577 (1991).

[85] T. P. Devereaux and D. Einzel, Phys. Rev. B **51**, 16 336 (1995).

[86] M. Palumbo and M. J. Graf, Phys. Rev. B **53**, 2261 (1996).

[87] H. Monien, K. Scharnberg, and D. Walker, Solid State Commun. **63**, 263 (1987).

[88] F. Carsey, R. Kagiwada, M. Levy, and K. Maki, Phys. Rev. B **4**, 854 (1971).

[89] L. S. Borkowski, P. J. Hirschfeld, and W. O. Putikka, Phys. Rev. B **52**, 3856 (1995).

[90] J. Bass, Adv. Phys. **21**, 431 (1972).

[91] G. Bergmann, Phys. Rev. B **3**, 3797 (1971); H. Takayama, J. Phys. (Paris) Suppl. **5**, C4-299 (1974); B. Keck and A. Schmid, Solid State Commun. **17**, 799 (1975).

[92] S. Quinlan, D. J. Scalapino, and N. Bulut, Phys. Rev. B **49**, 1470 (1994).

[93] L. J. Buchholtz and G. Zwicknagl, Phys. Rev. B **23**, 5788 (1981).

[94] H. Monien, K. Scharnberg, L. Tewordt, and D. Walker, Solid State Commun. **61**, 581 (1987).

[95] D. Walker, Master's thesis, Universität Hamburg, 1986.

[96] P. J. Hirschfeld, P. Wölfle, and D. Einzel, Phys. Rev. B **37**, 83 (1988).

[97] G. Preosti, H. Kim, and P. Muzikar, Phys. Rev. B **50**, 1259 (1994).

[98] Y. Sun and K. Maki, Phys. Rev. B **51**, 6059 (1995).

[99] P. Arberg, M. Mansor, and J. P. Carbotte, Solid State Commun. **86**, 671 (1993).

[100] S. Lenck and J. P. Carbotte, Phys. Rev. B **49**, 4176 (1994).

[101] P. J. Hirschfeld and N. Goldenfeld, Phys. Rev. B **48**, 4219 (1993).

[102] H. Kim, G. Preosti, and P. Muzikar, Phys. Rev. B **49**, 3544 (1994).

[103] P. Lee, Phys. Rev. Lett. **71**, 1887 (1993).

[104] A. J. Berlinsky, C. Kallin, G. Rose, and A.-C. Shi, Phys. Rev. B **48**, 4074 (1993).

[105] D. van der Marel, M. Bauer, E. H. Brandt, H. U. Habermeier, D. Heitmann, W. König, and A. Wittlin, Phys. Rev. B **43**, 8606 (1991).

[106] J. Münzel, A. Zibold, H. P. Geserich, and T. Wolf, Europhys. Lett. **33**, 147 (1996).

[107] H. B. G. Casimir and J. Ubbink, Philips Tech. Rundsch. **28**, 204 (1967).

[108] D. A. Bonn, Kuan Zhang, S. Kamal, Ruixing Liang, P. Dosanjh, W. N. Hardy, C. Kallin, and A. J. Berlinsky, Phys. Rev. Lett. **72**, 1391 (1994).

[109] J. C. Swihart and D. Shaw, Physica **55**, 678 (1971).

[110] P. B. Allen, W. E. Pickett, and H. Krakauer, Phys. Rev. B **37**, 7482 (1988).

[111] C. T. Rieck and K. Scharnberg, Physica B **163**, 670 (1990).

[112] C. T. Rieck, K. Scharnberg, S. Hensen, and G. Müller, J. Low Temp. Phys. **105**, 503 (1996).

[113] O. M. Froehlich, H. Schulze, R. Gross, A. Beck, and L. Alff, Phys. Rev. B **50**, 13 894 (1994).

[114] O. M. Froehlich, A. Beck, R. Gross, H. Saito, and M. Naito (unpublished).

[115] C. T. Rieck (unpublished).

[116] K. Holczer, O. Klein, and G. Grüner, Solid State Commun. **78**, 875 (1991).

[117] M. L. Horbach and W. van Saarloos, Phys. Rev. B **46**, 432 (1992).

[118] S. Kamal, D. A. Bonn, N. Goldenfeld, P. J. Hirschfeld, Ruixing Liang, and W. N. Hardy, Phys. Rev. Lett. **73**, 1845 (1994).

[119] S. T. Anlage, J. Mao, J. C. Booth, D. H. Wu, and J. L. Peng, Phys. Rev. B **53**, 2792 (1996).

[120] A. A. Golubov, M. R. Trunin, S. V. Shulga, D. Wehler, J. Dreibholz, G. Müller, and H. Piel, Physica C **213**, 139 (1993).

[121] H. K. Olsson and R. H. Koch, Physica C **185-189**, 1847 (1991); N. E. Glass and W. F. Hall, Phys. Rev. B **44**, 4495 (1991).

[122] C. Varmazis, J. R. Hook, D. J. Sandiford, and M. Strongin, Phys. Rev. B **11**, 3354 (1975).

[123] C. Varmazis, Y. Imry, and M. Strongin, Phys. Rev. B **13**, 2880 (1976).

[124] J. J. Gannon, Jr., B. S. Shivaram, and D. G. Hinks, Europhys. Lett. **13**, 459 (1990).

[125] P. J. C. Signore, B. Andraka, M. W. Meisel, S. E. Brown, Z. Fisk, A. L. Giorgi, J. L. Smith, F. Gross-Alltag, E. A. Schuberth, and A. A. Menovsky, Phys. Rev. B **52**, 4446 (1995).

[126] P. J. Hirschfeld, W. O. Putikka, P. Wölfle, and Y. Campbell, J. Low Temp. Phys. **88**, 395 (1992).

[127] E. J. Nicol and J. P. Carbotte, in *Studies of High Temperature Superconductors*, edited by A. Narlikar (Nova Science, New York, 1993), Vol. 11, p. 225.

[128] P. J. Hirschfeld, J. Phys. Chem. Solids **56**, 1605 (1995).

[129] M. J. Graf, M. Palumbo, D. Rainer, and J. A. Sauls, Phys. Rev. B **52**, 10 588 (1995).